SUB-NANOSECOND INFRARED OPTICAL PARAMETRIC PULSE GENERATION IN PERIODICALLY POLED LITHIUM NIOBATE PUMPED BY A SEEDED FIBER AMPLIFIER

Matthew D. Cocuzzi

Electro-Optical Countermeasures Technology Branch
Electro-Optical Sensor Technology Division

FEBRUARY 2008
Interim Report

STINFO COPY

AIR FORCE RESEARCH LABORATORY
SENSORS DIRECTORATE
WRIGHT-PATTERSON AIR FORCE BASE, OH 45433-7320
AIR FORCE MATERIEL COMMAND
UNITED STATES AIR FORCE

NOTICE AND SIGNATURE PAGE

This report was cleared for public release by the Wright-Patterson Air Force Base (WPAFB) Public Affairs Office and is available to the general public, including foreign nationals. Copies may be obtained from the Defense Technical Information Center (DTIC) (http://www.dtic.mil).

AFRL-RY-WP-TR-2008-1033 HAS BEEN REVIEWED AND IS APPROVED FOR PUBLICATION IN ACCORDANCE WITH ASSIGNED DISTRIBUTION STATEMENT.

*//Signature//

KENNETH L. SCHEPLER, Principal Scientist
EO CM Tech Branch, EO Sensor Tech Div
Sensors Directorate

//Signature//

JOHN F. CARR, Chief
EO CM Tech Branch, EO Sensor Tech Div
Sensors Directorate

//Signature//

BRIAN C. FORD, Col, USAF
Chief, EO Sensor Technology Division
Sensors Directorate

This report is published in the interest of scientific and technical information exchange, and its publication does not constitute the Government's approval or disapproval of its ideas or findings.

*Disseminated copies will show "//Signature//" stamped or typed above the signature blocks.

REPORT DOCUMENTATION PAGE				*Form Approved* *OMB No. 0704-0188*
The public reporting burden for this collection of information is estimated to average 1 hour per response, including the time for reviewing instructions, searching existing data sources, searching existing data sources, gathering and maintaining the data needed, and completing and reviewing the collection of information. Send comments regarding this burden estimate or any other aspect of this collection of information, including suggestions for reducing this burden, to Department of Defense, Washington Headquarters Services, Directorate for Information Operations and Reports (0704-0188), 1215 Jefferson Davis Highway, Suite 1204, Arlington, VA 22202-4302. Respondents should be aware that notwithstanding any other provision of law, no person shall be subject to any penalty for failing to comply with a collection of information if it does not display a currently valid OMB control number. **PLEASE DO NOT RETURN YOUR FORM TO THE ABOVE ADDRESS.**				

1. REPORT DATE *(DD-MM-YY)* February 2008	2. REPORT TYPE Interim	3. DATES COVERED *(From - To)* 01 August 2006 – 31 December 2007	
4. TITLE AND SUBTITLE SUB-NANOSECOND INFRARED OPTICAL PARAMETRIC PULSE GENERATION IN PERIODICALLY POLED LITHIUM NIOBATE PUMPED BY A SEEDED FIBER AMPLIFIER		**5a. CONTRACT NUMBER** In-house	
		5b. GRANT NUMBER	
		5c. PROGRAM ELEMENT NUMBER 62204F/61102F	
6. AUTHOR(S) Matthew D. Cocuzzi		**5d. PROJECT NUMBER** 2003	
		5e. TASK NUMBER 12	
		5f. WORK UNIT NUMBER 20031224	
7. PERFORMING ORGANIZATION NAME(S) AND ADDRESS(ES) Electro-Optical Countermeasures Technology Branch (AFRL/RYJW) Electro-Optical Sensor Technology Division Air Force Research Laboratory, Sensors Directorate Wright-Patterson Air Force Base, OH 45433-7320 Air Force Materiel Command, United States Air Force		**8. PERFORMING ORGANIZATION REPORT NUMBER** AFRL-RY-WP-TR-2008-1033	
9. SPONSORING/MONITORING AGENCY NAME(S) AND ADDRESS(ES) Air Force Research Laboratory Sensors Directorate Wright-Patterson Air Force Base, OH 45433-7320 Air Force Materiel Command United States Air Force	Air Force Office of Scientific Research (AFOSR) 875 N. Randolph Street Arlington, VA 22203-1768	**10. SPONSORING/MONITORING AGENCY ACRONYM(S)** AFRL/RYJW	
		11. SPONSORING/MONITORING AGENCY REPORT NUMBER(S) AFRL-RY-WP-TR-2008-1033	

12. DISTRIBUTION/AVAILABILITY STATEMENT
Approved for public release; distribution unlimited.

13. SUPPLEMENTARY NOTES
Report contains color. This is the author's Master's thesis through the University of Dayton's Electro-Optics program.
PAO Case Number: WPAFB 07-0643, 05 Dec 2007.

14. ABSTRACT
A ytterbium-doped, polarization maintaining PM double-clad fiber was seeded at one end and pumped at the other end, using dichroic filters to protect the pump and seed lasers, creating a fiber amplifier. The seed laser was a passively Q-switched Nd:YAG microchip laser operating at 1064 nm, polarized 99:1, 7.14 kHz repetition rare, 0.5 nsec pulse width, average power of 38 mW, and 5.3 µJ pulse energy. The pump laser was a 915 nm diode laser coupled to a fiber pigtail, operating at a maximum of 6 W with 7 A of operating current. The 3.56-m-long FC connectorized fiber was the active element and had a 25 µm core diameter and a 248 µm inner cladding diameter with 400-µm-diameter spliced silica end-caps to prevent damage polished at 8° to prevent back reflections. The PPLN crystal was an uncoated 1 x 14 x 49-mm-long multigrating crystal with approximate parallelism of the front and back surfaces. The domain grating period used was 29.5 µm, converting the 720 mW (over 100 µJ pulse energy) fiber amplifier beam to a 1.507 µm signal beam and a 3.619 µm idler beam, with 24% of the pump energy going to the signal and idler outputs.

15. SUBJECT TERMS
Nonlinear Optics, Fiber Optics, Periodically Poled Materials, Solid-State Lasers, Semiconductor Lasers, Ytterbium Doped Fiber, Polarization Maintaining Fiber

16. SECURITY CLASSIFICATION OF:			17. LIMITATION OF ABSTRACT: SAR	18. NUMBER OF PAGES 94	19a. NAME OF RESPONSIBLE PERSON (Monitor) Kenneth L. Schepler
a. REPORT Unclassified	**b. ABSTRACT** Unclassified	**c. THIS PAGE** Unclassified			19b. TELEPHONE NUMBER *(Include Area Code)* N/A

Standard Form 298 (Rev. 8-98)
Prescribed by ANSI Std. Z39-18

Abstract

Sub-Nanosecond Infrared Optical Parametric Pulse Generation in Periodically Poled Lithium Niobate Pumped by a Seeded Fiber Amplifier

Matthew D. Cocuzzi
University of Dayton

Advisor: Dr. Peter E. Powers

In this experiment, a ytterbium-doped fiber was seeded at one end and pumped at the other end, using high-performance dichroic filters to protect both the pump and the seed lasers, thus creating a fiber amplifier. The seed laser was a passively Q-Switched Nd:YAG microchip laser operating at 1064 nm, polarized 99:1, 7.14-kHz repetition rate, 0.5-nsec pulse width, average power of 38 mW, and 5.3 µJ pulse energy. The fiber amplifier was pumped at 915 nm using a diode laser which was coupled to a fiber pigtail and operated at a maximum of 6 W with 7 A of operating current. An Yb^{3+}-doped, panda-structure, polarization maintaining (PM), double-clad fiber was the active element and had a 25-µm core diameter and a 248-µm inner cladding diameter. The fiber was 3.56 m long and FC connectorized; 400-µm diameter silica end-caps were spliced to it to prevent damage and polished at 8° to normal to prevent back reflections. The fiber operated at a maximum average power of 720 mW with over 100 µJ pulse energy.

The PPLN crystal was a 1-mm x 14-mm cross-section x 49-mm long multigrating crystal with no coatings and approximate parallelism of the front and back surfaces. The domain grating period used was 29.5 µm, converting the fiber amplifier beam to a 1.507 µm signal beam and a 3.619 µm idler beam, with 24% of the pump energy going to the signal and idler outputs.

Table of Contents

List of Illustrations

List of Tables

Acknowledgements

This thesis project would not have been possible without the continued assistance, advice, and support of many people. First and foremost I thank my advisor, Dr. Peter Powers, for his unlimited enthusiasm and creative solutions to problems. I would also like to thank Dr. Kenneth Schepler for all of the insight and support he provided. Special thanks go out to Professor Ivan T. Lima, Jr., for his continued collaboration and suggestions.

Additional thanks are especially in order for Mr. Patrick Berry, for the constant assistance and suggestions he provided throughout the course of this project. Also, I would like to thank Dr. Rita Peterson, Mr. Scott Lewis, and Lt. Timothy Calver for the assistance and training they provided when I was working on specific equipment. I would like to thank Mr. James Alverson for creating a custom MATLAB program to determine M^2 values by curve-fitting, and for all of the suggestions and ideas he provided throughout the project.

Most importantly, I thank my wife, Kim, for her unwavering support and encouragement. Without her, none of this would have been possible.

Chapter 1
Introduction

1.1 Motivation

The use of periodically poled lithium niobate (PPLN) as the nonlinear medium for Optical Parametric Generation (OPG) has been studied thoroughly in recent years, largely as a result of high nonlinearity (d_{33} = 27pm/V) [1], especially when pumped by high-peak-power pulsed lasers [2,3,4]. Continued development has led to commercially available polarization-maintaining fibers doped with rare-earth elements, allowing the fiber to be an active element rather than simply a waveguide. The use of erbium fiber amplifiers to pump PPLN [5,6], along with improvements in ytterbium-doped fiber amplifiers [7,8], have benefited from bending-losses that induce single mode operation in a multimode fiber [9]. Fiber amplifiers can eliminate the necessity for free-space optics (lenses and mirrors separated by air), a trait that complements the small footprint, rugged structure, and lack of free-space optics in semiconductor lasers.

Many communications and sensing applications operate in the infrared and, as such, there is an increasing desire for a high-power infrared source that can be mounted in land and air vehicles. Current high-power lasers in the

infrared regions require both an active cooling source and internal free-space optics, and can be very expensive [10].

An initial solution is semiconductor lasers as they are relatively inexpensive, have no free-space optics, and require no active cooling system. Semiconductor lasers, such as diode lasers, and solid state lasers such as passively Q-switched microchip lasers, also have a very small footprint, thus allowing greater options of where the laser is mounted, and are rugged enough to endure environments considered too harsh for most lasers – environments such as temperature changes (*e.g.* a plane taking off from the ground and moving to high-altitude) or vibration (*e.g.* a truck driving on a gravel road). However, semiconductor lasers tend to have low beam quality (*e.g.* diode lasers), while microchip lasers can have low average power.

Combining the high-power from diode lasers with the high beam-quality of microchip lasers requires an active element, such as erbium or ytterbium, to act as a gain medium. Erbium Doped Fiber Amplifiers (EDFAs) have been used by the telecommunications industry for nearly 20 years [11,12] to simultaneously amplify a high-quality beam (generally a data-stream) and act as a waveguide. Recently, other rare-earth elements have been used as dopants in optical fibers. In the case of this project, the optical fiber is doped with ytterbium as it has absorption and emission bands that fit the wavelength requirements of the project. Recent studies have shown ytterbium-doped fiber operating at high

average power with picosecond pulses[13] and high peak power at sub-nanosecond pulses[14].

With an established starting point of a high-quality beam guiding through an active fiber that is pumped by a high-power beam, referred to as a fiber amplifier, the remaining dilemma is to obtain the wavelength required. Nonlinear devices, such as Optical Parametric Oscillators (OPO) and Optical Parametric Generators (OPG), provide the capability to convert the wavelength of light that passes through the device, and have been studied for nearly 40 years[15]. However, OPOs and OPGs require a polarized beam, which requires either polarizing the output of the fiber amplifier at the expense of power or a means of preserving the polarization of the microchip laser beam as it propagates through the fiber. Polarization maintaining fibers, doped with an active element, have become commercially available and are the last step in providing an infrared source that is rugged, has a small footprint, is relatively inexpensive, requires no cooling system, and has no free-space optics.

1.2   Project Background

This project began as an experiment by a visiting professor from North Dakota State University, Professor Ivan T. Lima, Jr., in the summer of 2006. At the end of his AFOSR Summer Faculty Fellowship, Professor Lima had built an initial fiber amplifier that produced a highly multimode output with 550 mW average power at 7 W of pump power (approximately 60 µJ/pulse). After very

3

tightly coiling the fiber, the fiber amplifier had an M^2 of 1.9 (see Section 2.4.1), but the attenuation from coiling the fiber reduced the output energy to approximately 28 µJ/pulse. The fiber amplifier output was focused into a PPLN crystal with the intent of activating OPG and generating a signal beam. However, the summer fellowship ended before the PPLN output could be examined for any signal generation.

This project continued the experiment to improve the fiber amplifier performance and demonstrate that the fiber amplifier successfully activated a PPLN OPG.

1.3 Overview of Thesis

Chapter 2 presents background information and theory regarding ytterbium doped fibers and their use in fiber amplifiers, connectorization of optical fibers, polarization maintaining fibers, Gaussian beams and the beam propagation factor M^2, and nonlinear optics specifically related to PPLN and OPG. Chapter 3 explains the process involved in the design and development of the fiber amplifier, including descriptions of all equipment used and tasks performed, and the results of the final fiber amplifier design. Chapter 4 details the setup and alignment of a PPLN crystal to function as an OPG, and the filtering and measurement of the result. Chapter 5 provides ideas and suggestions for future work that could utilize or improve upon either the fiber amplifier or the entire fiber amplifier PPLN OPG system. Appendix A is all of the MATLAB code used throughout the project. Appendix B contains a paper that was submitted to

and accepted by the Optical Society of America (OSA) Advanced Solid-State Photonics (ASSP) conference in Nara, Japan, scheduled for January 27-30, 2008.

Additionally, references will be noted by a superscript with brackets with page numbers listed after a semicolon, *e.g.*[123:12-34], MATLAB code will be referenced by a superscript with brackets and an M[M123].

Chapter 2
Theory and Background

2.1 Yb^{3+} Fiber Amplifier

A fiber amplifier consists of a fiber with an active element dopant (typically a rare-earth element such as erbium (Er) or ytterbium (Yb)) which is pumped by a high-power laser with a wavelength in an absorption band of the dopant and seeded by a high-beam-quality laser with a wavelength in the emission band of the dopant. In the case of this project, the dopant was ytterbium, which had an absorption and emission spectrum as shown below in Figure 1, with absorption peaks at 920 nm and 976 nm and emission peaks at 976 nm and 1030 nm[8]. The desired fiber amplifier output was 1064 nm (within the emission band) and, as diode laser wavelength can change as a function of temperature, a pump laser at 915 nm was selected such that the pump source would remain in the absorption band.
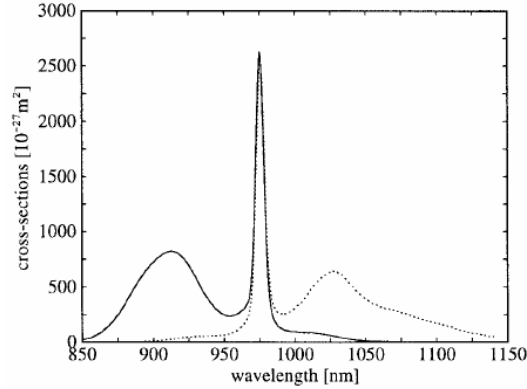
Figure 1: Ytterbium Absorption (solid) and Emission Spectrum (dashed) [8]

While it is certainly possible to find high power lasers at 1064 nm, there are two immediate benefits of a fiber amplifier over traditional free-space lasers: there are few (if any) free-space optics, providing a fiber amplifier with much greater environmental resilience, and a fiber amplifier has a small, flexible footprint which allows a fiber amplifier to be placed in a variety of positions unsuitable for standard lasers. In this project, the pump laser is a diode laser of dimensions 17.5mm x 21mm x 6.5mm and the seed laser is a microchip laser of dimensions 30mm x 35mm x 140mm, whereas typical mode-locked or Q-switched lasers are large (*e.g.* 1840mm x 482mm x 229mm [16]), expensive, and require an active cooling system[10]. This project uses free-space optics to couple the pump and seed lasers into and out from the fiber to allow greater flexibility in the event of a change in the system design, though Wavelength Division Multiplexers with connectorized ends could be employed to do the coupling once the system was adequately refined. With the elimination of free-space optics, the effect of vibration on the laser would be greatly reduced and sensitivity to temperature change would be minimal.

7

As with any propagating fiber, it is vitally important to know how many modes will propagate. This is calculated from the following equations[17], where a is the core diameter, λ is the propagating beam wavelength, NA is the numerical aperture, V[17] is the V-Number, and M is the number of modes:

$$a = 25\,\mu m \quad \lambda = 1.064\,\mu m \quad NA = 0.07$$

$$V = \frac{2\pi a}{\lambda} NA = 10.33 \tag{1.}$$

$$M \approx \frac{V^2}{2} = 53 \tag{2.}$$

With approximately 53 propagating modes, pulse energy is spread over the beam cross-section and changes as the beam propagates. As such, there is the possibility that the fiber amplifier output could successfully and efficiently pump a nonlinear device, but that is unlikely. Single mode operation is desired as all of the energy in the pulse would be in a single, central spot that doesn't dramatically change as the beam propagates. Reducing the number of modes guided by a fiber generally entails selecting a fiber with single-mode characteristics (a V-parameter less than 2.405[18]) provided by a rather small core radius – on the order of 5 µm. Another option is spooling the fiber around two orthogonal spools, which can be built in the lab with anything from mounting posts to cardboard tubes[19]. However, there are two significant results from tightly spooled fiber that can impair the progress of an experiment. First, tightly spooling a fiber places extreme stress on the fiber, which can lead to breakage either immediately from over-bending or later as a result of the reduced structural integrity of the spooled fiber. The second significant hindrance is the loss of

power associated with "bending losses" which reduces the amount of single-mode power is available as the higher-order modes are attenuated, thus decreasing the performance of the spooled fiber as a pump for a nonlinear device. A solution that reduces the existence of higher order modes, without the bending loss or residual stress on the fiber associated with spooling, is mode-matching an incident beam as it couples into the fiber.

2.2   Connectorization

Connectorizing a fiber requires a connectorizer with a bore diameter the size of the fiber diameter, a protective boot, and a drop or two of epoxy – an example of the boot and connectorizer, along with a connectorizer schematic [20], are shown below in Figure 2.
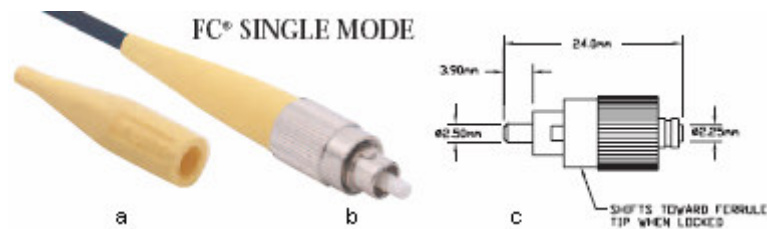
Figure 2: Fiber Connectorizer Boot (a), Boot and Connectorizer (b), and Connectorizer Diagram (c)

The boot is slipped over the fiber and the protective jackets removed by carefully stripping the jacket with a razor blade, soaking the fiber tip in alcohol or paint thinner to dissolve the jacket, or by quickly running the fiber through an open flame. The fiber is then cleaned by soaking a paper towel in alcohol and wiping the bare (jacketless) fiber. Generally, a drop of epoxy is placed in the center of the connectorizer and the fiber pushed through the connectorizer,

cleaved, and pulled back until only the very tip of the fiber protrudes from the connectorizer with a small bead of epoxy (see Figure 3 below). This drop of epoxy holds the fiber tip in place at the tip of the connectorizer, which reduces the possibility that the fiber tip will move if the connectorizer bore isn't exactly the same diameter as the bare fiber.
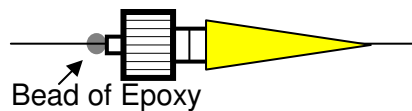
Bead of Epoxy

Figure 3: Front Tip Bead of Epoxy

In this project, this bead of epoxy on the connectorizer will be exposed to high power (approximately 7 Watts) focused to approximately 100µm, which can cause the epoxy to melt, burn, or vaporize and attach to the fiber tip. As a result, this drop of epoxy that is normally placed inside the connectorizer is ignored for this project. With or without the bead of epoxy at the tip of the fiber, the boot is then attached to the connectorizer using either epoxy or a crimper (or both), and a small drop of epoxy glues the fiber to the tail-end of the boot. The notch in the FC Connector ensures that, when mounted to a connectorized mount, the fiber always has the same orientation (especially important in polarization-maintaining fibers) and the same transverse location and position along the optic axis. Shown in Figure 4 below is an FC mount adapter for a 1" lens mount and a close-up of the notch.
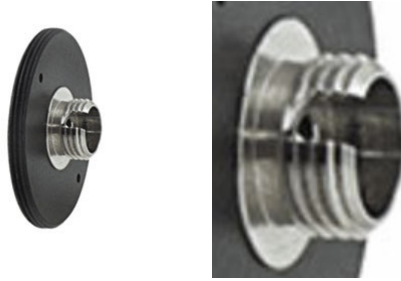
Figure 4: FC Connectorizer Adapter (left), Notch Close-up (right)

Connectorizing provides key benefits to a fiber amplifier system including stability, repeatability, and protection. With the fiber fixed in place within an appropriate connectorizer (one with a bore diameter equal to the fiber diameter), the fiber will not move when under adverse conditions such as mechanically-induced vibration (such as airplane turbulence) or heat-induced movement caused by high pump power. Additionally, a connectorized fiber can be removed from the fiber amplifier system and a new fiber can be inserted into the system with minimum adjustments required, which simplifies the maintenance of the fiber amplifier. The fiber also receives a certain amount of protection from the connectorizer as the bare fiber end should never be exposed more than 1 mm from the connectorizer (as opposed to other fiber mounting systems which generally expose 10 mm of bare fiber), thus reducing the chances of damaging the cleaved or polished end.

2.3   Polarization Maintaining Fibers

Polarization-Maintaining Fibers will maintain the polarization of a beam if the beam is coupled correctly through the use of birefringence induced by stress

rods[21]. The stress rods can be aligned in a number of ways, two of the most common of which are Bowtie and Panda. Additionally, Photonic Crystal Fibers can be polarization-maintaining by using larger-than-average-diameter airholes[22] to effectively act as stress rods. Shown below in Figure 5 are crosscuts of each type listed above[23,24,25].
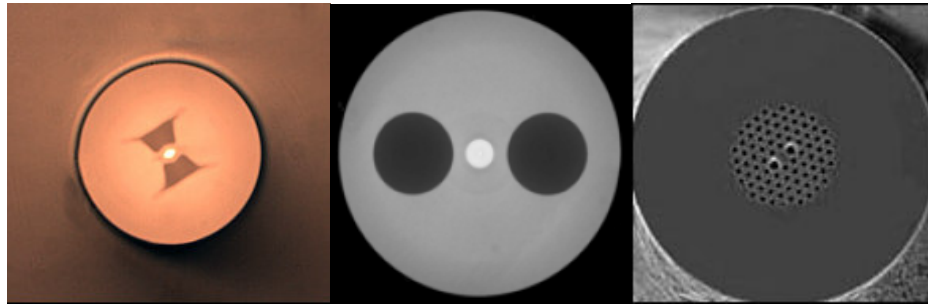
Figure 5: Polarization Maintaining Fibers: Bowtie (left), Panda (center), Photonic Crystal (right)

Polarization maintaining fibers present an additional challenge to the goal of perfect alignment if the fiber is connectorized in such a way that the FC connector notch forces the stress rods to be misaligned to the incoming beam polarization, or if future changes to the configuration of the fiber amplifier system affect the polarization of light coupling into the fiber. For this potential problem, two solutions exist. The more complex solution is to use FC connectors with an Adjustable Key, such as the ThorLabs Adjustable Key Connector, which can be rotated about the optic axis to adjust for any alignment issues. The simpler solution to the problem of alignment is to use a half-wave plate to rotate the incident laser beam, which trivializes any PM fiber-connector misalignment. A second half-wave plate allows the fiber amplifier output beam to be rotated without adjusting the fiber itself. Additionally, the half-wave plate option does not

share the potential problem of translational movement that can arise if the bore in the Adjustable Key Connector is not exactly centered in the connector.

2.4 Gaussian Beams

Gaussian beams have been studied extensively for over 40 years[26], resulting in well-known equations to calculate the parameters of a beam propagating through a medium, a lens, and a flat or curved surface, and incident upon a flat or curved mirror. These equations can be found in many sources including Silfvast's Laser Fundamentals: Second Edition[27:404-405,424-427], Yariv and Yeh's Photonics[28:68-69,79-85], and Saleh and Teich's Fundamentals of Photonics[29:28-30,82-83], and are dependant on the complex beam parameter, q, defined as given below in Equation 3:

$$q = z + q_0 = z + jz_0 \tag{3.}$$

where z is the distance from the minimum radius of the Gaussian beam along a propagation path, called the beam waist, and z_0 is the Rayleigh range, defined in Equation 4 as:

$$z_0 = \frac{\pi w_0^2}{\lambda} \tag{4.}$$

where w_0 is the beam waist. The Rayleigh range is especially useful because optimal focusing through a crystal is achieved when the crystal is approximately twice as long as the Rayleigh range.

The two most pertinent parameters of a Gaussian beam at a given point are the beam radius and the radius of curvature of the wave-front. The equations governing the beam radius and the radius of curvature are presented (respectively) in Equation 5 and Equation 6.

$$w^2(z) = w_0^2 \left(1 + \left(\frac{z}{z_0} \right)^2 \right)^2 \tag{5.}$$

$$R(z) = z \left(1 + \left(\frac{z}{z_0} \right)^2 \right) \tag{6.}$$

From these equations, the q-parameter equation is derived to its final form, shown in Equation 7:

$$\frac{1}{q} = \frac{1}{R(z)} - j \frac{\lambda}{\pi w^2(z)} \tag{7.}$$

To propagate the q-parameter, the following (Equation 8 [M1,M2]) is used in either form:

$$q_2 = \frac{A q_1 + B}{C q_2 + D} \quad \text{or} \quad \frac{1}{q_2} = \frac{C + D/q_1}{A + B/q_1} \tag{8.}$$

where A, B, C, and D refer to the *ABCD* ray-trace matrices. The propagation of the q-parameter is simplified through the *ABCD* matrices shown in Table 1.

Table 1: ABCD Matrices

Description	ABCD Matrix
Thin lens [M2] focal length *f*	$\begin{bmatrix} 1 & 0 \\ -1/f & 1 \end{bmatrix}$
Curved surface Surface radius *R* new index of refraction n_2 old index of refraction n_1	$\begin{bmatrix} 1 & 0 \\ \frac{n_1 - n_2}{R * n_2} & \frac{n_1}{n_2} \end{bmatrix}$

Flat surface new index of refraction n_2 old index of refraction n_1	$\begin{bmatrix} 1 & 0 \\ 0 & \dfrac{n_1}{n_2} \end{bmatrix}$
Medium [M1] index of refraction n propagation distance d	$\begin{bmatrix} 1 & d/n \\ 0 & 1 \end{bmatrix}$
Curved mirror radius of curvature R	$\begin{bmatrix} 1 & 0 \\ -2/R & 1 \end{bmatrix}$
Flat mirror	$\begin{bmatrix} 1 & 0 \\ 0 & 1 \end{bmatrix}$

A common method to determine an initial q-parameter is to place a lens in the beam path and measure the beam radius at various positions after the lens and fitting the data to the beam waist equation (Equation 5) to determine the beam waist. At the beam waist, the distance from the beam waist, z, is zero, so the initial q-parameter is found from Equation 9 [M3,M4] to be:

$$q = jz_0 = j\frac{\pi w_0^2}{\lambda} \tag{9.}$$

Another method for defining the initial q-parameter is to assume a beam to be perfectly collimated. A collimated beam has a radius of curvature of infinity (the beam is not expanding) and all points will be minima (and thus a "beam waist"), so the initial q-parameter will have the same result as the above. With the initial q-parameter determined, the q-parameter anywhere along the beam path can thus be calculated.

2.4.1 M-squared

The M^2 term is used to calculate beam divergence of a real beam compared to a perfect Gaussian and is always greater than one, as an M^2 equal

to one would be a perfect TEM_{00} Gaussian beam. That is to say, a real beam is M^2 *times* a perfect Gaussian beam, which will "give a rigorous and very useful measure of how the beam will propagate through free space or indeed through any kind of paraxial optical system," [30] and is commonly referred to as the beam's "quality." To calculate the M^2 value of a beam, the beam radius is measured and fit to a modified beam radius equation, shown below in Equation 10[27:425] [M5]:

$$W^2(z) = W_0^{\ 2} + M^4 \frac{\lambda^2}{\pi^2 W_0^{\ 2}} (z - z_0)^2 \qquad (10.)$$

2.5   PPLN OPG

Optical Parametric Generation (OPG) is a nonlinear process which converts the energy from an incident beam into two lower-energy, longer wavelength beams. The incident beam is referred to as the pump beam, and the pair of generated beams are referred to as the signal and idler, where the signal beam has greater photon energy (and a shorter wavelength) of the two and is the beam that the OPG process is generally designed to generate. In this sense, the OPG process can be thought of as Sum Frequency Generation (SFG) in reverse except that the signal and idler beams can be any two wavelengths that fulfill the requirements described below. The origin of the signal and idler beams, in the absence of a "seed," is a phenomenon called parametric fluorescence, described by Sutherland as "quantum fluctuations … equivalent to the presence of ½ photon in both the signal and idler modes … or one photon in either mode."[31]

16

The derivation of the OPG process to the Coupled-Amplitude equations has been shown in many textbooks and will not be reproduced here, though the resulting equations are shown below in Equation 11[32].

$$\frac{dA_1}{dz} = j\frac{8\pi d_{eff}\omega_1^2}{k_1 c^2} A_3 A_2^* e^{-j\Delta kz}$$

$$\frac{dA_2}{dz} = j\frac{8\pi d_{eff}\omega_2^2}{k_2 c^2} A_3 A_1^* e^{-j\Delta kz}$$

(11.)

Additionally, understanding certain concepts from the derivation of the coupled-amplitude equations is fundamental to this project. The first such concept is that the interaction between the three beams must adhere to both the Conservation of Energy and the Conservation of Momentum, given in Equations 12 and 13, respectively.

$$\hbar\omega_p = \hbar\omega_s + \hbar\omega_i$$

(12.)

$$\hbar\vec{k}_p = \hbar\vec{k}_s + \hbar\vec{k}_i$$

(13.)

where the subscripts $p, s,$ and i refer to the pump, signal, and idler, and $\hbar$ is Planck's Constant divided by 2π. From the Conservation of Energy arises the fundamental wavelength relationship between the pump, signal, and idler, shown in Equation 14 [M6]:

$$\frac{1}{\lambda_p} = \frac{1}{\lambda_s} + \frac{1}{\lambda_i}$$

(14.)

There are two important concepts resulting from the above equation. The first such concept is that the above equation applies to all possible three-wave

17

interactions. That is, the initial pump beam energy is converted to the signal and idler beams. The other important result is that the signal and idler beams are not inherently defined as single values: just as a pair of dice has multiple combinations resulting in a sum of 7, multiple combinations of signal and idler beam frequencies will sum to the pump beam frequency. This means that the signal and idler will have some bandwidth. The magnitude of the bandwidth is determined by phasematching as described below.

The Conservation of Momentum ensures that the sum of the phases of the signal and idler beams is equal to the phase of the pump beam, where **k** is a 3-dimensional vector called the wave number, with a magnitude of:

$$k = \frac{2\pi n(\lambda)}{\lambda} \qquad (15.)$$

where $n(\lambda)$ is the Sellmeier equation describing refractive index as a function of wavelength (dispersion) for the particular nonlinear material in which the OPG process occurs. When the Sellmeier equation for the nonlinear material used does not result in k-vectors that fit the Conservation of Momentum equation with any pair of wavelengths calculated through Equation 16 (from the Conservation of Energy), the signal and idler beams do not experience any significant gain. The wave vector mismatch Δk is the same as in the phase component, $e^{-j\Delta kz}$, in the coupled amplitude equations mentioned previously, and is defined as:

$$\Delta \vec{k} = \vec{k}_p - \vec{k}_s - \vec{k}_i \qquad (16.)$$

To match the wave vectors is to match the phase of the beams and is thus called Phase Matching. In Quasi-Phase Matching (QPM), a nonlinear crystal is

engineered such that changing from one domain to the next produces a change in the sign of the nonlinear coefficient. In this project, the nonlinear material is Lithium Niobate (LiNbO₃), to which a template mask with a periodic pattern is applied via photolithography. The period applied is referred to as the "poling period" or the "grating period." An electric field applied to the lithium niobate sample then reverses the crystal orientation based on the mask pattern, thus becoming Periodically Poled Lithium Niobate (PPLN)[1]. A new Δk term for QPM is defined in Equation 17 (where *m* is an integer). When the grating period Λ_g satisfies Equation 18, the phases will be matched:

$$\Delta k_{QPM} = k_p - k_s - k_i - k_g$$
$$\text{where } k_g \equiv m\frac{2\pi}{\Lambda_g} \tag{17.}$$

$$m\frac{2\pi}{\Lambda_g} = k_p - k_s - k_i \tag{18.}$$

Understanding that the system is Quasi-Phase Matched when Δk_{QPM} equals zero allows the above equations to be entered into any mathematics software, along with the corresponding Sellmeier equations to define the refractive index. This, in turn, allows a user to enter the known data – generally the grating period and the pump laser wavelength – and yield the conditions of phase-matching: the signal and idler wavelengths. Other processes, such as the mixing of the pump and signal, pump and idler, SHG of the signal, etc., are all evident but at much lower energies because they are not phase-matched.

A benefit critical to the success of this project and work with Lithium Niobate as a whole is that the poling axis is the axis with the greatest nonlinearity coefficient, d, which increases the efficiency of any nonlinear process. As mentioned in the introduction, Lithium Niobate has a maximum d-coefficient of 27 pm/V [1], the nonlinear d-effective of which is 17 pm/V.

In order to approximate whether or not the pumped PPLN will produce a measurable OPG output, the required signal output power from the PPLN crystal is arbitrarily determined to be 1% of the crystal pump power. Equation 18[33] was used to calculate the OPG threshold, where K is defined, $I_{p,t}$ is the threshold intensity, L is the crystal length, λ_s is the signal wavelength, $E_{s,t}$ is the threshold signal power, h is Planck's constant, c is the speed of light in vacuum, d_{eff} is the effective nonlinear d-coefficient, ε_0 is the permittivity of free space, λ_i is the idler wavelength, and $n_{p,s,i}$ is the index of refraction for the pump, signal, and idler.

$$KI_{p,t} = \left[\frac{1}{2L}\ln\left(\frac{4\lambda_s E_{s,t}}{hc}\right)\right]^2$$

$$where: K = \frac{8\pi^2 d_{eff}^2}{\varepsilon_0 c \lambda_s \lambda_i n_s n_i n_p}$$

(19.)

2.5.1 OPG Threshold Calculation

The threshold calculation is presented as follows, assuming a crystal thickness of 1 mm and a crystal length of 4.9 cm, with a threshold detection power of 2.25mW:

$$KI_{p,t} = \left[\frac{1}{2*(4.9cm)} \ln\left(\frac{4(1.5\mu m)(2.25mW)}{(6.626\times10^{-34})(3\times10^{8})} \right) \right]^{2} = 16.291$$

$$K = \frac{8\pi^{2}(17\times10^{-12})^{2}}{(8.854\times10^{-12})(3\times10^{8})(1.5\mu m)(3.619\mu m)(2.155)(2.138)(2.072)} = 1.69\times10^{-7}$$

$$\therefore I_{p,t} = 96.1MW/cm^{2}$$

$$I_{p,t} = 96.1MW/cm^{2} = \frac{X_{th}(Watts)}{\pi*(radius)^{2}}$$

$$Crystal\ Length = 2z_{R} = 2\left(\frac{\pi w_{0}^{2}}{\lambda} \right)$$

$$49mm = \frac{2\pi w_{0}^{2}}{1.064\mu m}$$

$$w_{0} = 91.1\mu m$$

$$X_{th} = \pi*(91.1\mu m)^{2}*96.1MW/cm^{2}$$
$$X_{th} = 25kW$$
$$X_{ave} = 25kW*.5n\sec*7.14kHz = 89.25mW$$

The result of the calculation indicates that the fiber amplifier should have enough power to activate detectable OPG if has 90mW of average output power.

Chapter 3
Fiber Amplifier Design and Description

3.1 Initial Design Decision

When setting up a fiber amplifier, the most important decision to make is whether the pump and seed lasers will be co-directional, coupling into the fiber from the same end of the fiber, or counter-directional, coupling into the fiber on opposite ends of the fiber. Co-directional propagation provides significant initial safety to both the pump and seed lasers but couples both beams into the fiber through the same optics, which can be damaging to the lasers if there are any significant back-reflections. Counter-directional propagation is dangerous for the pump and seed lasers because the beams are literally pointing at each other, but allows the two beams to couple through their own optics, thus allowing ideal coupling for both beams. A diagram of the two setup options is shown in Figure 6, below. In this project, the pump laser beam only needs to couple into the cladding and has the potential to create heat-induced damage to the fiber if too-tightly focused (because instead of guiding down the fiber, the high-angle rays exit into the cladding where the power is absorbed and causes problems); counter-directional propagation was selected for this fiber amplifier experiment.

This chapter is organized by presenting various fiber-designs to show the route to optimizing the fiber laser system. Presented at the end are the conclusions and the lessons learned.
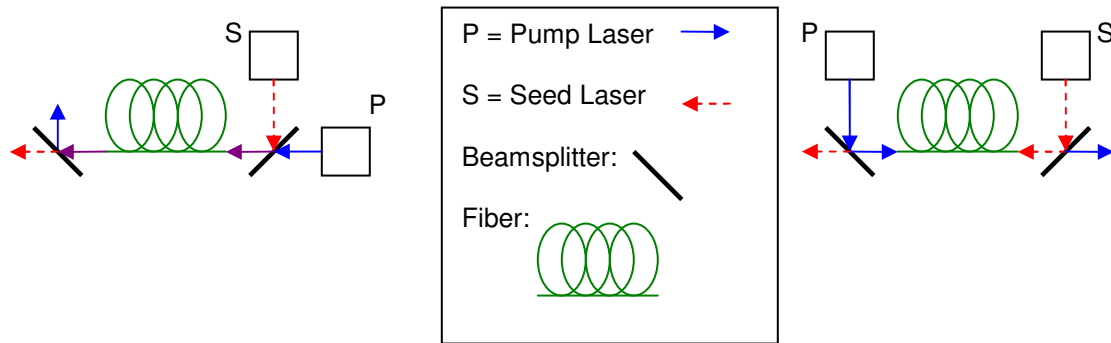
Figure 6: Fiber Amplifier Options: Co-Propagating (left), Legend (center), Counter-Propagating (right)

3.2   Equipment

The **Pump Laser** was a 915-nm diode laser from EM4, Inc., with a fiber pigtail, numerical aperture 0.22, and peak output power of 7 W with 8 A of operating current. The output power of the pump laser was measured at room temperature on two dates with respect to operating current, a graph of which is shown below in Figure 7. The plot indicates no degradation in performance over the course of the experiments.
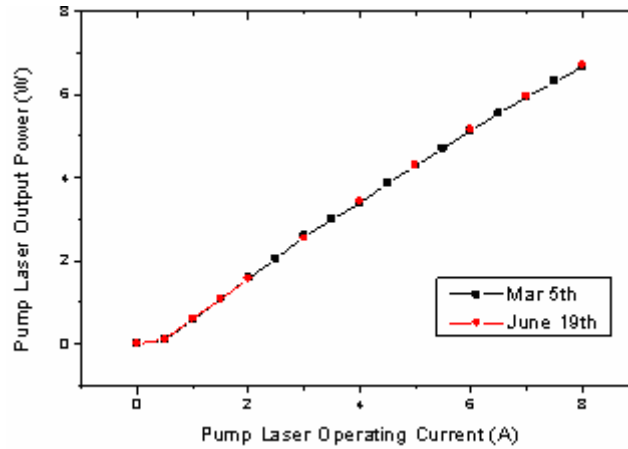
Figure 7: Pump Laser Output Power vs. Operating Current

The **Seed Laser** was a passively Q-switched Nd:YAG microchip laser from Teem Photonics which produced 1064-nm, 0.5-ns pulses at a repetition rate of 7.14 kHz. The average power of the seed laser was 38 mW with 5.3 μJ/pulse.

The **Active Fiber** used in this project was 3.56-m long, double-clad, polarization-maintaining (PM), large mode-area, and ytterbium-doped, manufactured by the Liekki Corporation, based out of Finland. The fiber properties are presented in Table 2 [24].

Table 2: Liekki Fiber Properties

Core Diameter	25 ± 2.5 μm
Cladding Diameter	250 ± 15 μm
Coating Diameter	350 ± 15 μm
Mode-field Diameter[1]	19.4μm

---

[1] Mode-field Diameter supplied via phone call to Liekki

Absorption at 920 nm	2.6 ± 0.7 dB/m
Core Numerical Aperture	0.07 ± 0.01

The other optics used in the fiber amplifier setup are listed in Table 3 below.

Table 3: Lenses, Mirrors, Isolator and Half-Wave Plates

Component Name	Key Parameter(s)
Isolator	1064 nm
RMI Dichroic Mirror x3	98% T @ 1064 nm, 98% R @ 915 nm
Seed Lens 1	f = 11 cm
ThorLabs C350TM-B	f = 4.5mm, NA = 0.41, radius = 4mm
ThorLabs C230TM-B	f = 4.5mm, NA = 0.55, radius = 4.5mm
OzOptics HPUCO-23-915-S-3.9AS-SP	f = 3.9 mm
Pump Lens 1	f = 100 mm
Pump Lens 2	F = 75.6 mm
OPG Focusing Lens	F = 88.3 mm

Note that the large core size of the fiber allows for high energy density propagation; however, it is not single mode. Getting a clean beam profile out of the fiber is addressed later in this chapter.

3.3 Initial Fiber Amplifier Setup
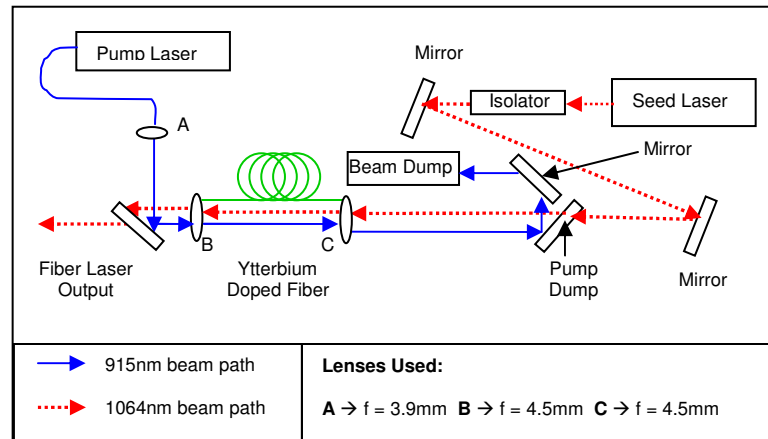
Figure 8: Initial Fiber Amplifier Setup

The initial design of the fiber amplifier is shown above in Figure 8. Three small base-plates were firmly mounted to the table and two 2" posts were connected and firmly mounted in the base-plates. The seed laser was mounted to a 7.5" by 7.5" plate, which was rigidly mounted to the posts – a detailed photograph can be seen in Figure 9 below. The seed laser was determined to be level by both observing the height of the beam on a ruler at several locations (through an IR Viewer scope) and checking the base-plate with a bubble level; no changes were deemed necessary.
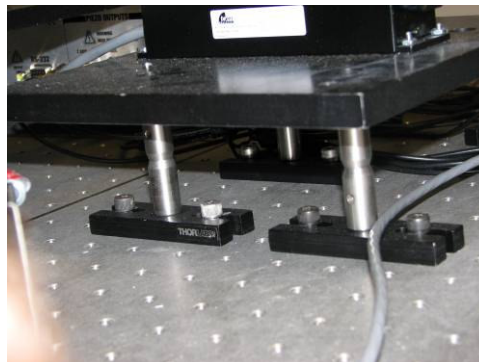
Figure 9: Details of Post-Supported Seed Laser Plate

With the seed laser level and rigidly mounted to the table, a beam dump was mounted approximately two feet away from the seed laser and an IR Viewer Scope was used to determine the position of the beam; this position was marked with a pencil. A 1064-nm isolator was placed approximately 10 cm from the seed laser and adjusted until the beam reached the same location as previously marked.

The stage used to mount the seed lens was a ThorLabs NanoMax® 311 nano-positioning stage with fixed differential drives and internal piezoelectric drives; this setup was used with an Open Loop piezo controller (ThorLabs MDT693A) to provide positioning resolution as fine as 1 µm manual adjustment and 20 nm piezo controlled adjustment. The NanoMax® was moved into position and mounted to the table with a ThorLabs HCS010 microscope lens adapter attached – no lens was mounted at this time. A dichroic filter to be used as a pump dump was inserted a few inches in front of the NanoMax® stage, at approximately the stage height; this filter was flat and did not affect focusing but did shift the beam path. Two silver mirrors were mounted to create an optic axis at the height of the NanoMax® stage using an iris after the dichroic filter and a ThorLabs HFS001 adapter on the stage. A silver mirror and BlackHole beam dump (Blue Sky Research) were set up in conjunction with the pump dump dichroic filter.

With the seed laser mounted and aligned, the pump laser was mounted to a 3" x 3" plate with a thermally conductive sheet between the laser and the plate. The plate was then mounted to the table. The pump laser's fiber pigtail had been connectorized previously by Professor Lima and was attached to the OzOptics fiber collimator. The collimator/pigtail arrangement was mounted on two translation stages transverse to the beam path (one vertical and one horizontal). The pump beam was guided to a Newport F19TS stage using another dichroic filter, mounted at the stage height. A beam dump was mounted between the two stages (where the fiber would later be placed) and the IR Viewer was used to guide the pump beam through the Newport stage to the beam dump where the beam location was marked as before with the seed laser.

At this point, the seed and pump coupling lenses were mounted to their respective stages. The seed coupling lens, a ThorLabs C350TM-B had a diameter of 8.2 mm and required a lens mount, a ThorLabs S1TM09, to be drilled and a set screw inserted – this altered the alignment of the seed laser, so the mirrors were adjusted until the output after the focusing lens was circular and centered at the same location along the beam path. The custom drilled seed lens mount is shown below in Figure 10 and was mounted to the microscope lens mount on the NanoMax® stage by a ThorLabs SM1A4 1"-to-microscope adapter. The pump laser focusing lens, a ThorLabs C230TM-B, was mounted to a ThorLabs E09RMS microscope lens adapter and had no alignment issues.
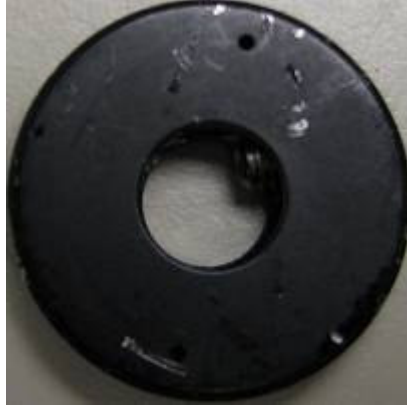
Figure 10: Custom Drilled Lens Mount with visible Set Screw

The fiber was spooled around two 1.5" diameter posts mounted at 90° to each other on a base-plate to induce bending losses that would reduce the existence of higher-order modes[34] and produce a higher quality output beam at the cost of overall output power, as demonstrated by Koplow, *et al.*[9]. This is necessary because of the large core size fiber used (which allows high energy density). The spool posts are shown below in Figure 11.
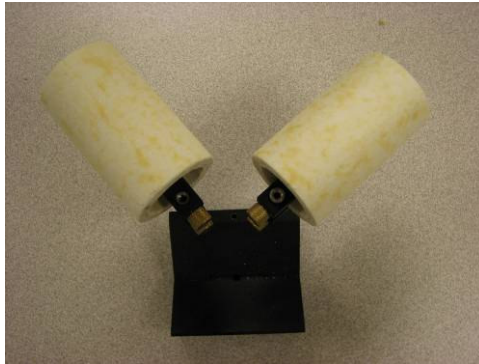
Figure 11: Fiber Spool Posts at 90° to Induce Bending Loss

The fiber ends were inserted through brass chucks and stripped of their jacket, cleaned with alcohol, and cleaved. Once cleaved, the fiber was slid back into the brass chuck so that only 1/2" of fiber was exposed. On both ends, a small piece of paper with a hole punched by a fine-tip pen was slid over the fiber

down to the brass chuck to be used with the IR viewer to help visually align the fiber to the incoming beams. Once the beams were roughly aligned from a distance, the brass chucks – mounted on the seed side by a ThorLabs HFS001 adapter on the NanoMax® stage and mounted on the pump side by a Newport FPR-1A adapter on the Newport stage – were slid to within the focal length of the fiber focusing lenses.

The pump laser was the first to be finely aligned to the fiber. The mirror redirecting the pump beam from the pump-dump dichroic was removed and a piece of paper was placed approximately two feet from the dichroic. The pump-side brass chuck was aligned using the Newport stage until a definite fiber image could be seen (with the IR Viewer scope) on the piece of paper. This image was optimized by minor adjustments of the Newport stage.

The seed-side brass chuck was moved along the beam axis until the pump beam produced a focused image of the fiber stress-rods, at which point the brass chuck was rotated until the stress rods were vertically aligned. This then set the polarization axes to be horizontal and vertical, which is convenient for the seed laser. The brass chuck was mounted in place so that it could not rotate and a piece of paper was placed leaning against the pump-dump dichroic. The seed laser was turned on and the NanoMax® stage was adjusted such that the pump beam and seed beam were concentric. The purpose of the focused stress-rod image was to ensure that the seed beam would focus extremely well into the

fiber with the understanding that the different wavelengths of the pump and seed lasers would require some minor adjustments to optimize seed focusing.

The minor adjustments for the seed side were performed by viewing the fiber output with the IR Viewer scope and increasing the pump power slightly. While examining the output image, the seed-side brass chuck was moved transversely about the beam axis until a very bright center spot appeared and was optimized.

3.4   Initial Design Results

The unpumped fiber amplifier output power was 15.8 mW total, with 3.8 mW in the core. Slowly pumping the fiber allowed measurements to be made regarding the fiber amplifier output power versus the pump power. Initially, the gain was a factor of 2 to 5, indicating that the pump-side chuck was misaligned. At low pump power, the brass chuck was moved to optimize the fiber amplifier output. The pump laser power was increased and the optimization was performed again. This continued until the pump laser was at approximately 5 A of pump operating current, or 4.3 W of pump power. At this point, the pump-side of the fiber visibly glowed a faint green (from up-conversion) – further pumping increased the intensity of the glowing. A few iterations of harder pumping and optimizing, the output power reached approximately 117 mW and immediately cut off. From that point on, no amount of pumping would produce any significant

gain. The pump laser output was measured and, with the pump operating current at its peak, the pump laser power was a mere 20 mW as opposed to the previous output of 4.3 W.

The pump laser was damaged by amplified seed laser pulses reaching the pump laser pigtail and guiding directly into the pump laser. The dichroic filter used to direct the pump beam into the fiber and let the amplified seed beam pass was tested – only 85% of the seed beam was transmitting, and at 117 mW of average power with 0.5-ns pulse width and 7.14-kHz pulse repetition rate, the peak power of the pulses was 32.7 kW, of which 27.8 kW was transmitted but 4.9 kW was coupled into the pump laser, burning out the diode. An image of a diode laser with Catastrophic Optical Damage (COD) is shown below in Figure 12.
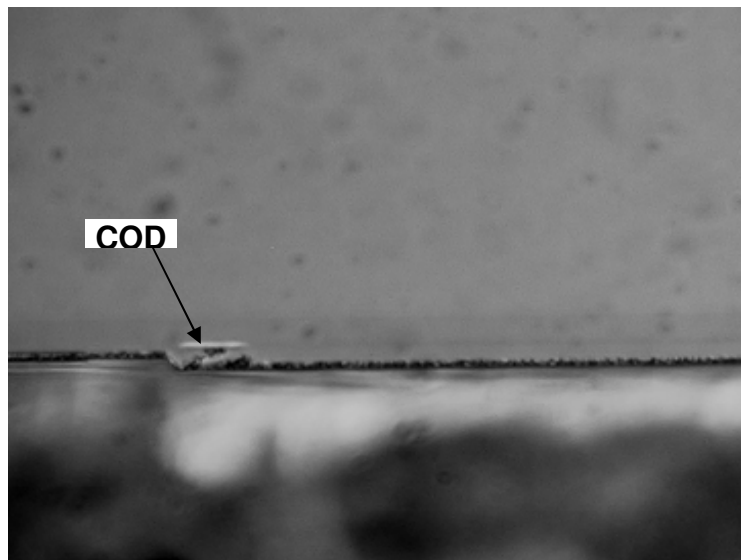
**Figure 12: Catastrophic Optical Damage (COD) on a Diode Laser**

3.5 Improved Design – Dichroics and Endcaps – and Results

New dichroic filters were ordered from RMI (Rocky Mountain Instrument Co.) which reflected 98% of the 915-nm pump beam and transmitted 98% of the 1064-nm signal beam – the data sent by RMI was verified in the lab using the Varian Cary® 5000 Spectrophotometer.

A new pump laser was re-positioned such that there were two dichroic filters to create an optic axis at the Newport stage height. From this point on, the pump laser was never damaged. A third RMI dichroic was used in the place of the original pump-dump dichroic to further protect the seed laser.

With the new filtering in place, the slightly-pumping/optimally-aligning process resumed, with a new interesting complication. When further pumping the fiber, the power would rise rapidly and slowly drift away over a span of about 5 seconds. The pump laser was turned up a great deal and, as soon as it was turned off, the power meter was removed so that the camera could see the fiber amplifier output. There was no visible output for a few seconds, and then the output image drifted into the screen and off the other side. This was caused by heat-induced bending of the ½" of protruding fiber, which had the potential of causing a great deal of inconsistency. After many iterations, the fiber amplifier output reached a measured peak of 230 mW and immediately shut down to almost nothing, though the actual output power could have been much higher due to the latency of power meters' reliance on heat measurements. The pump

laser was measured at various operating currents and was found to be fully operational; the seed laser was operating normally as well. The fiber amplifier output was viewed with the IR Viewer scope and had absolutely no pattern to it whatsoever. The decision was made to break the end off of the fiber to inspect it under a high power microscope; the resulting images (from the end and the side views) are shown below in Figure 13.
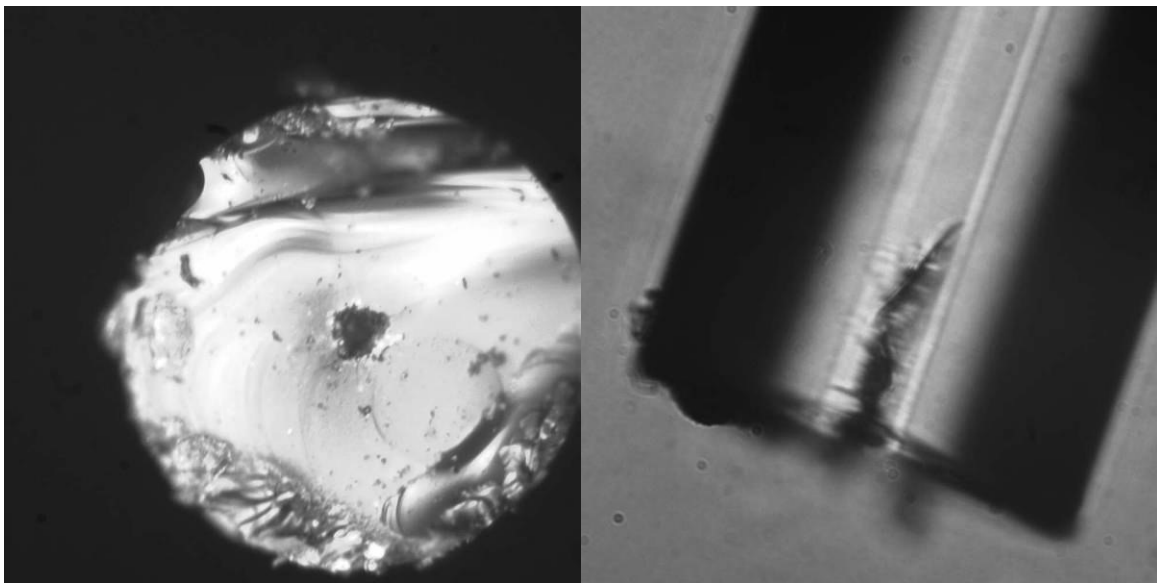
Figure 13: Fiber End Intensity Damage – End View (left) and Side View (right)

Unsure as to what exactly happened, a chance meeting with Dr. Mark Bowers and Dr. Fabio Di Teodoro, both from Aculight Corporation, led to an in-depth discussion about fiber amplifier design. From this discussion, the previous damage to the fiber was understood to be a result of the fully-pumped 1064-nm beam intensity at the fiber surface. Assuming 225 mW average power, the intensity at the surface of the fiber was calculated as shown below.

Fiber: 19.4µm mode-field diameter (9.7µm radius)
Fully-Pumped Fiber Amplifier Output: 225mW at 7.14kHz pulse rate, 0.5ns pulse width

$$225mW = .225W = .225\frac{\text{Joules}}{\text{sec}}$$

$$.225\frac{\text{J}}{s} = 7140\frac{\text{Pulses}}{\text{s}} * X\frac{\text{J}}{\text{Pulse}}$$

$$X = 31.5\frac{\mu J}{\text{Pulse}}$$

$$X\frac{\text{J}}{\text{Pulse}} * \frac{1}{0.5}\frac{\text{Pulse}}{\text{nanosecond}} = 63kW \text{ peak power}$$

$$I = \frac{\text{Power}}{A} = \frac{63000W}{\pi*(9.7\mu m)^2} = 21.31\frac{GW}{cm^2}$$

While the bulk damage threshold of silica fibers is 50 GW/cm^2 [35,36], the surface damage threshold is much lower: approximately 7.3 GW/cm^2 [35]. Without limiting the pump power, the only way to reduce the intensity at the fiber surface is with a fiber end-cap. The theory behind the end-cap is that a large-core-diameter non-doped silica fiber is spliced onto an active fiber and cleaved just long enough to allow the beam to expand from the size of the core diameter of the active fiber to the size of the large core of the end-cap, a diagram of which is shown in Figure 14 below – the surface is at an angle as end-caps are generally polished at 8° to prevent back-reflection. Using fiber end-caps for this project, the intensity would be reduced a great deal (by a factor of 425), as shown in the calculation below.

$$I_{endcap} = \frac{\text{Power}}{A} = \frac{63000W}{\pi*(200\mu m)^2} = 50.13\frac{MW}{cm^2}$$
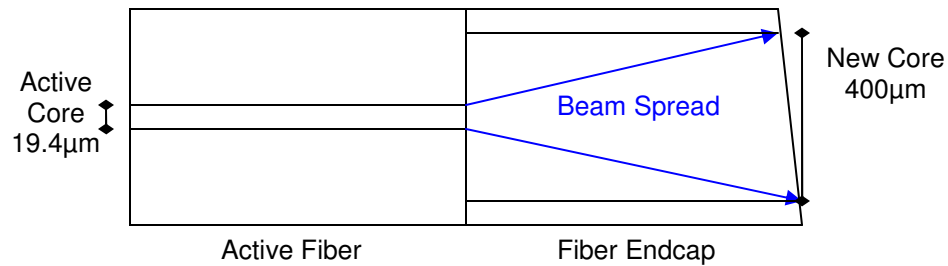
Figure 14: Diagram of Fiber Endcap

This reduction in intensity prevented the blow-out effect shown previously in Figure 13. Additionally, because the end-capped fiber would be connectorized (to help protect the end-cap), there would be no heat-related bending.

Dr. Bowers said that Aculight could perform the end-cap splicing if needed; thus the decision was made to make an in-house spliced end-cap and compare it to a professionally produced end-cap. A section of fiber was sent to Aculight and another section of fiber was taken to the University of Dayton Electro-Optics laboratory; unfortunately the local equipment could only handle fibers with a maximum diameter of 100 µm: less than half the diameter of the fiber for this project.

3.6   *Further Improvements – Mode-Matching*

While waiting for the Aculight fiber, the entire fiber amplifier setup was re-examined to find potential improvements. The initial coupling of the seed beam was immediately questioned and changed. A ThorLabs HFB003 FC

connectorized adapter was ordered to mount the seed coupling lens to the NanoMax® stage. A ThorLabs RMS08 (microscope-to-8mm lens adapter) was ordered to provide a connectorized mount for the fiber on the NanoMax® stage and was placed on the track on the NanoMax® stage and slid along the beam path to help re-align the axis formed by the two silver mirrors. With the axis aligned and the lens in place, a razor blade was attached to the NanoMax® stage and the beam was profiled using the knife-edge technique, in which the beam diameter is determined at a position along the beam path by measuring the transverse points where the beam intensity drops to 92% and 8% of the peak [30,37]. The setup of the knife-edge profile is shown in Figure 15 below.
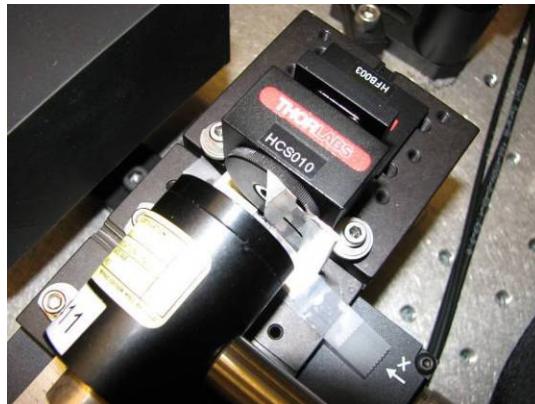
Figure 15: Knife-Edge Profile - Razor Blade on NanoMax Stage

In Professor Lima's initial design, the seed laser was coupled into the fiber by simply matching the Numerical Aperture (NA) of the fiber and the coupling lens. The NA-matching method deals exclusively with the acceptance angle of the fiber and the incident angle of the beam, which is a viable technique for diodes (such as LEDs) or large-core-diameter fiber. However, the very small core-diameter of the fiber and the Gaussian nature of the beam are incompatible

with the NA-matching technique if highly efficient, precise coupling is desired. Mode-matching was used in this case to produce a very low-order (if not single-mode) propagating beam with high efficiency.

The knife-edge profile data was fit to the Gaussian beam waist equation through the use of custom MATLAB code [M7]. The initial measurements showed that the beam size was not matched to the 19.4 µm fiber mode. However, this fit determined a Gaussian q-parameter that allowed for a calculation of the beam before the focusing lens. With this information, various lenses were virtually inserted along the beam path to produce a beam waist diameter as close to 19.4 µm as possible – this resulted in an f = 11 cm lens placed 10 cm from the seed coupling lens. The beam was profiled using the same knife-edge arrangement as in Figure 15 and the results are shown below in Figure 16. A minor adjustment to improve the mode-matching was made by moving the 11-cm lens 0.5 cm further away from the seed-focusing lens, resulting in a calculated beam waist radius of 8.15 µm, or a diameter of 16.3 µm, very close to the mode-field diameter of the fiber – the data and curve, shown in Figure 17, don't overlap at the beam waist as the beam was focused tightly enough to drill through the razor blade, thus artificially increasing the distance between the 92% and 8% points.
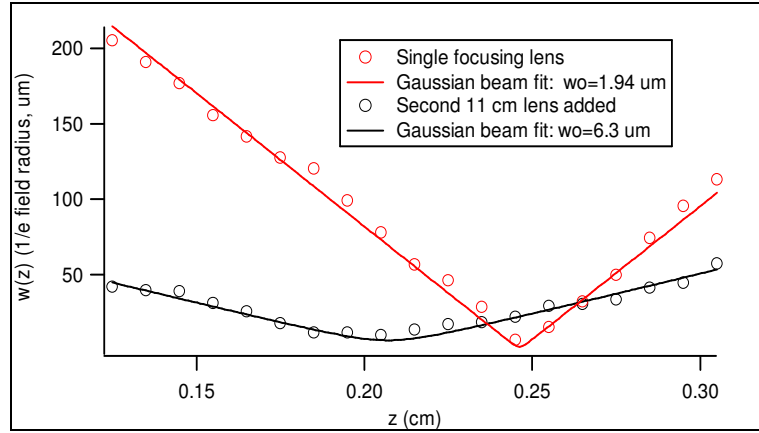
Figure 16: Seed Laser Beam Profile with and without 11cm Lens
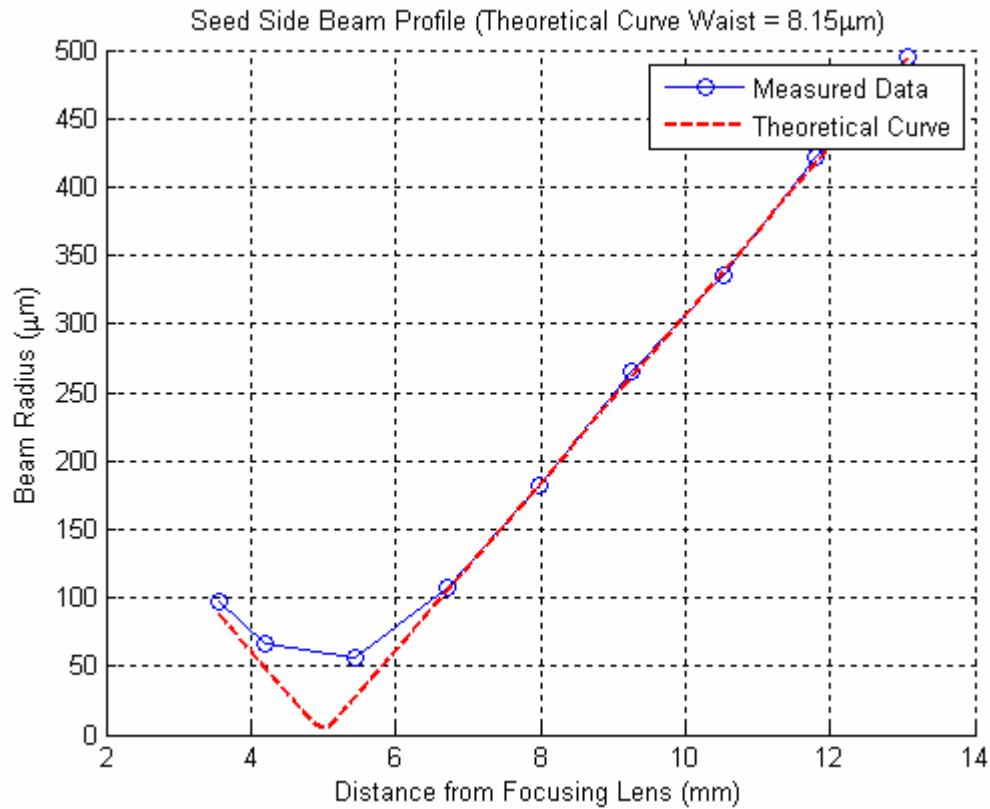

**Figure 17: Seed Laser Mode-Matching Measurement and Curve Fit**

The pump side of the fiber received similar treatment. The beam location was marked on a beam dump mounted where the fiber was previously located. In the case of the pump laser, the beam didn't need to be perfectly mode-matched to the core: the pump beam only needed to be focusing into the much larger

cladding. This was especially important as the exact distance from the lens to the fiber would be determined by collimating the amplified seed laser output. Therefore, to ideally couple the pump beam into the inner cladding of the fiber, three beams were modeled in MATLAB. The first beam that was modeled was called the Target beam in this project, and was defined as being collimated at the fiber with a diameter of 100μm. This was back-calculated through the focusing lens to determine what focusing would be necessary to produce a collimated output from the focusing lens. The second beam was called the Actual beam, which was measured using the knife-edge technique and back-calculated to the pump laser collimating lens. The third beam was called the Solution beam, which used the at-the-pump-laser result from the Actual beam as a starting point. By inserting and moving lenses and propagating the Solution beam to the fiber, a very close approximation to the Target beam was achieved.

All three of these virtual beams are shown below in Figure 18: the Target beam is blue, the Actual beam is black and dashed, and the Solution beam is red and dotted[M7]. A detailed view of the pump coupling at the fiber is shown in Figure 19[M8].

Beam Profile Back Calculations
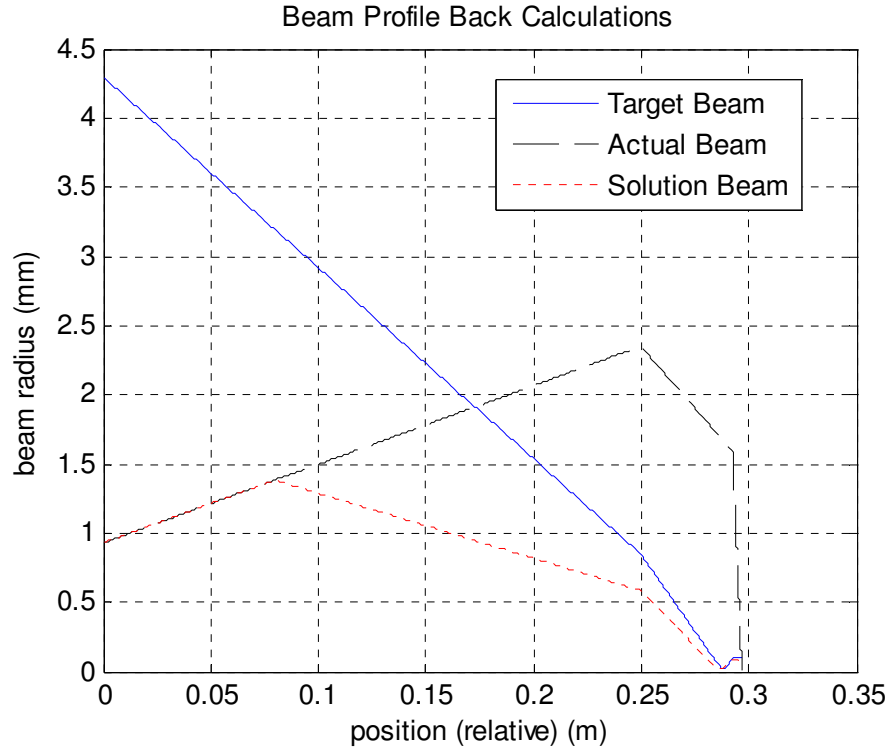
Figure 18: Pump Beam Back Calculations and Desired Adjustments

Beam Radius Along Pump Beam Path
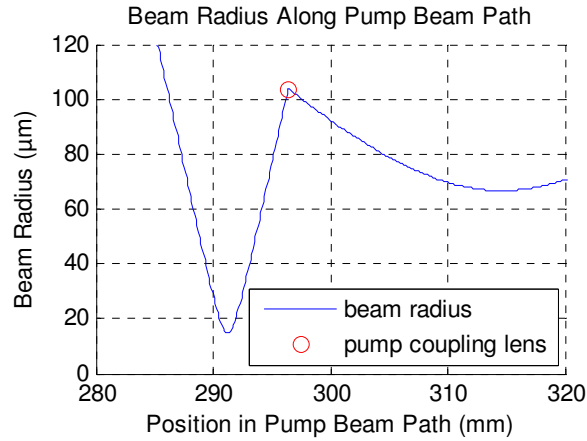
Figure 19: Pump Laser Mode-Matching Calculation

After a few simulations, a final lens configuration was developed. The lenses, an f = 100 mm lens and an f = 75.6 mm lens, were placed in the pump beam path at their respective locations, detailed in Figure 20 below, by mounting the lenses to translation stages that moved along the beam axis
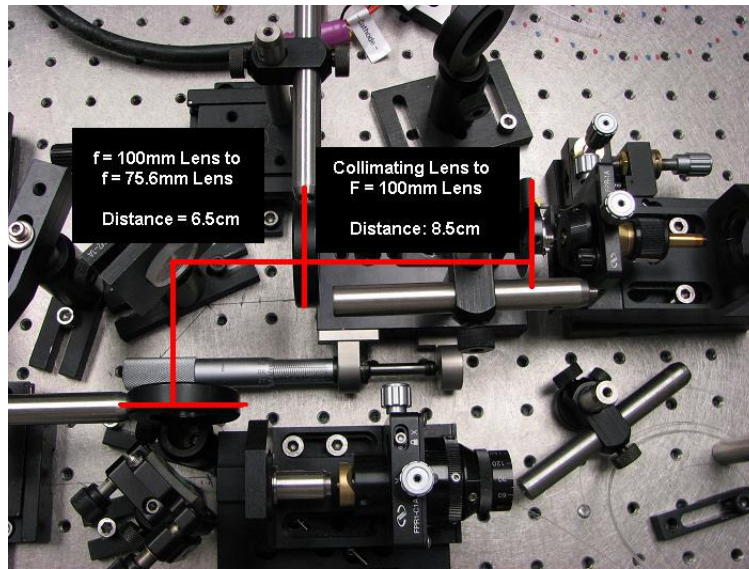
Figure 20: Pump Focusing Lenses and Separation Distances

Using two 4" posts and a 90° bracket, the lenses were moved transversely to the beam path until the beam reached the position marked on the beam dump. Adjustments were made with the translation stages to minimize the pump beam spot size at the beam dump, verifying that the pump beam coming out of the pump focusing lens was slowly approaching collimation. Note that the focused spot size (radius) range of 80-100µm closely matches the 125µm cladding radius.

3.7 Fiber Preparation and Connectorization

The next step, after notification was received that the Aculight-prepared fiber was finished, was to connectorize the fiber in-house to do preliminary alignment. Connectorizers with a bore of the same diameter (or slightly larger) as the fiber were ordered from ThorLabs. The fiber was slid through the boot of the

connectorizer and stripped of its jacket. The fiber was cleaned in alcohol and slowly pushed through the connectorizer. When just barely enough fiber was through the connectorizer to fit in the cleaver, the fiber was cleaved, examined from the side with the fiber microscope for flatness, and pulled back in the connectorizer such that approximately 0.5mm of fiber protruded from the connectorizer. At this point, the fiber was examined with the fiber microscope again from the end to determine the overall cleanliness of the cleave. If the fiber wasn't cleanly cleaved, it would be re-cleaved and re-examined; if the fiber was clean, it would be fixed in place. Normal connectorization is performed by first inserting a drop of epoxy in the connectorizer before inserting the fiber [38], which would be detrimental in this project because the high-power pump laser would either melt, burn, or vaporize the epoxy at the fiber tip. Instead, after the fiber was examined and only 0.5 mm of the fiber protruded from the connectorizer, a drop of epoxy was placed on the fiber where the end of the fiber boot will be located and a drop of epoxy was placed on the connectorizer where the boot would be affixed to the connectorizer; these locations are shown in Figure 21 below. The boot was then slid to the connectorizer and needle-nose pliers were used to crimp the boot to the epoxy on the connectorizer, the tail of the boot was dabbed into the epoxy on the fiber, and the epoxy was given a few hours to cure. This process was performed on both ends of the fiber.
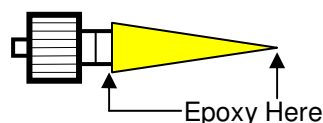
Figure 21: Fiber Connectorizer Epoxy Location for High-Power Systems

With the fiber connectorized and inserted into the system, the pump laser was slowly turned on and the fiber amplifier output was measured. As the pump laser power increased, the pump coupling was adjusted to maximize the output power. As the pump laser power reached approximately 5 W, the fiber amplifier output began to slowly decrease and the connectorizer started to smoke. The pump and seed lasers were immediately turned off, though the damage had already been done; the epoxy at the connectorizer boot had absorbed enough light either guiding along the outer cladding or escaping, both of which are artifacts of poor alignment. Shown below are images of the connectorizer and boot (Figure 22, left) and the epoxy damage on the fiber (Figure 22, right).
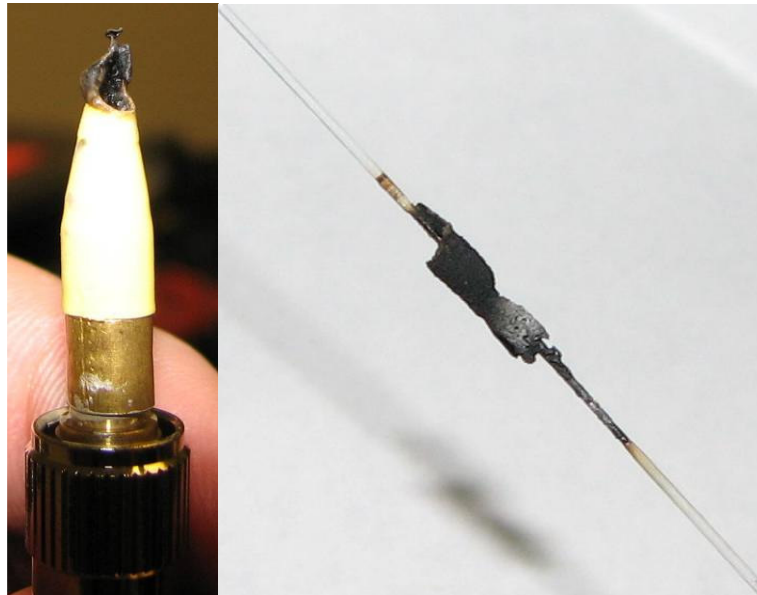
Figure 22: Misalignment Damage – Connectorizer Boot (left) and Epoxy (right)

The fiber was cleaved and re-connectorized, this time without any epoxy so that, in the event of further damage, only a minimal amount of the fiber would have to be discarded.

3.8   In-House Connectorized Fiber System

A Newport FPHCA FC-Collimator Brass Chuck was mounted on the Newport stage using a Newport FPR1-C1A mount and the ThorLabs HFB003 was already in place on the NanoMax® stage. The in-house fiber was attached to the connectorized mounts, which were then moved as close as possible to the focal point of the lenses given the degree of accuracy required. The seed beam was turned on and a camera was used to observe the fiber amplifier output. When the seed beam was adequately coupling through the fiber, an output image was observed on the camera, example photographs are shown below in Figure 23 – one of the entire output, one of only the core.

Figure 23: Camera Aided Alignment: Entire Output (left), Core Output (right)

The pump side of the fiber was then moved along the beam path to focus the output image and rotated such that the stress rods were vertically aligned. The seed side was then moved, scanning the transverse plane at various points along the beam path, until a very bright center spot was observed which saturated the camera if it was not attenuated. The seed side was continually

adjusted, trying to maximize the center spot. This consisted of translating the fiber along the beam direction slightly, peaking up the transverse alignment, and repeating the whole process again until the optimum z-position was found. The fiber tip was moved along the beam axis to each of the points where the bright central spot was no longer observable, determining a center point for the fiber tip, where the tip was then moved. At this position, the center spot was at an assumed peak – though it did not appear to be any different from the center spot in other positions along the beam path. The entire unpumped fiber amplifier output power at this stage was 16 mW, of which 4 mW was in the core.

Various attempts to find the "sweet spot" were made without success. In an attempt to try something outside the normal bounds, the seed laser alignment mirrors were adjusted while observing the center spot on the camera. With a strong neutral density filter absorbing the output, the center spot was only slightly visible. When the alignment mirrors were tweaked, the center spot saturated almost instantly. The output was measured again, finding that of the 16-mW output, 9 mW was contained within the core. At this point, the fiber amplifier design was complete, a diagram of which is presented in Figure 24 below.
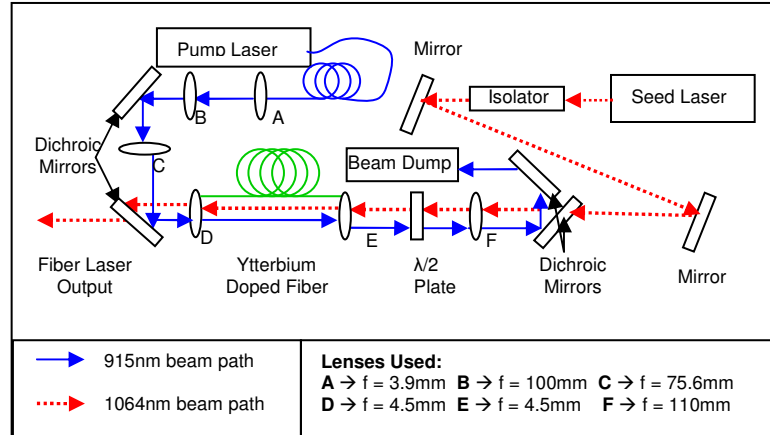
Figure 24: Fiber Amplifier Setup – Microchip seed laser pulses at 1064 nm are amplified in an ytterbium-doped, polarization maintaining fiber. The fiber amplifier is pumped by a 915-nm diode laser.

The power meter was repositioned and the fiber amplifier was turned on using an iris to only examine the output power in the core of the fiber. The pump laser power versus pump laser operating current was again measured: it exactly overlapped the measurements from a few months prior. The core output power was measured versus the pump laser operating current but plotted versus the pump laser power, as shown below in Figure 25. The amount of power measured prior to the fiber end damage (Figure 13) was approximately 230 mW, so the fiber amplifier output was kept below 200 mW while further optimizing to prevent damage.
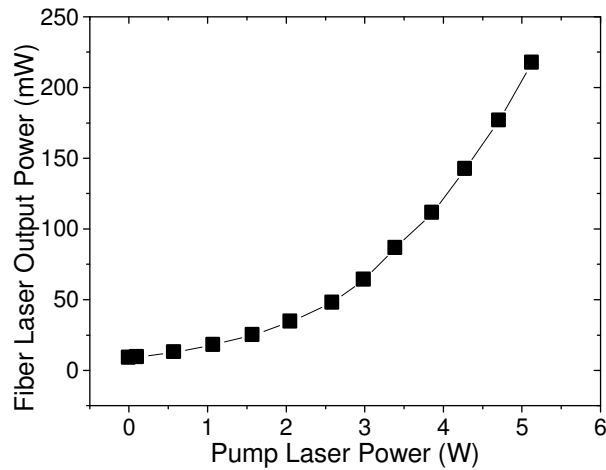
Figure 25: Fiber Amplifier Output Power vs Pump Laser Power -- In-House Fiber

3.9 Fiber Amplifier with Aculight-prepared Fiber

The fiber prepared by Aculight was swapped into the fiber amplifier and pumped slowly: the pump operating current was raised in 250 mA increments every 10 to 15 seconds, until reaching 5 A of pump operating current. This was done to ensure that the fiber was properly aligned before reaching high pump power operation. The fiber amplifier output power was almost immediately a significant improvement over the fiber prepared in-house. The final output power of the fiber amplifier, using the Aculight-prepared fiber, was measured with respect to pump power and is shown below in Figure 26. The measured power peaked at 720 mW with 6 W of pump power, which correlates to 7 A of pump operating current. While the diode pump laser can operate at 8 A of pump

operating current, the pump laser begins to heat very rapidly at that current and can burn out if it runs too hot for too long.
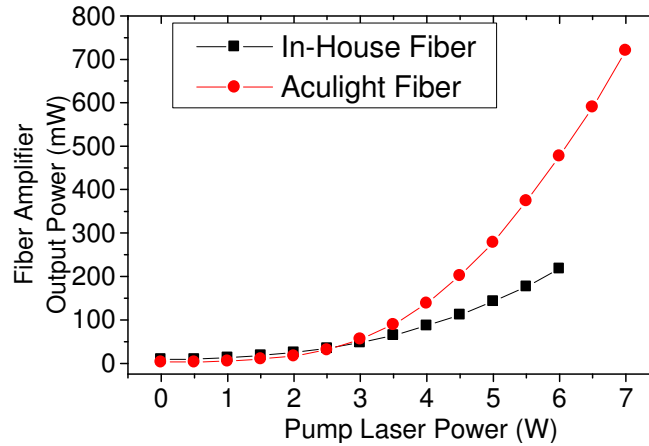
Figure 26: Fiber amplifier Output: Average Output Power vs Pump Laser Power

The pump laser beam was calculated to have 96% coupling efficiency into the fiber with 8% assumed loss on uncoated lenses and 2% measured loss on the dichroic mirrors (see Table 3). The seed laser beam coupled into the fiber at 56% efficiency, calculated by dividing the fiber throughput power by its input power. Shown below in Figure 27 is the pulse shape of the beam after passing through the fiber, measured by directing the fiber output to a 1.5 GHz Newport 818-BB-30A[39] InGaAs (rise time and fall time < 400psec) detector which was connected to a 2 GHz (10GSamples/sec) LeCroy 204Xi Waverunner[40] oscilloscope.
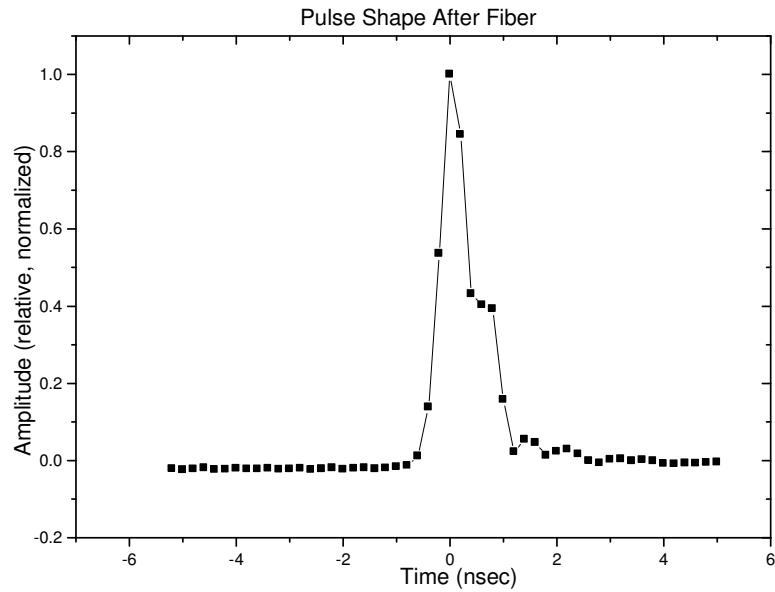
Figure 27: Fiber Output Pulse Shape (unpumped).

The fiber amplifier output was measured using a NanoScan® beam profiler from Photon, Inc., to determine the (beam quality/beam propagation factor) M^2 in the X and Y axes. The NanoScan® hardware had two software packages -- NanoScan® Software, which operated the NanoScan® detector head and provided various methods of examining the detected beam, and ModeScan® Software, which used the measurements from the NanoScan® Software to automatically calculate the M^2 in X and Y directions. Use of the ModeScan® Software was quite simple: 10 positions along the beam path were indicated and the NanoScan® head measured the beam at those points. However, the M^2 calculated from these measurements was 0.2, which is not physically possible. After making several changes in the measurement method, from scanning frequency to operation in Pulsed Laser mode, the results were the same. Manual beam profiling was performed with the NanoScan® measuring

data at the same point along the beam path, leading to a factor of 1.36 between the manual measurement and the automatic measurement. It should be noted that literature available on the Photon, Inc website indicates that the NanoScan® is not recommended for use with certain combinations of repetition rate and beam waist[41], as the system was designed for continuous-wave beams, and number of pulses measured during one rotation of the scanning drum will not reach the 16 required by ISO standards.

After the automatic data was adjusted by this factor, a custom MATLAB function, written by Mr. Jim Alverson[M5,M9], fit the data to a Gaussian beam waist curve, from which the M^2 value of the fiber amplifier beam was calculated: the M^2 factors were determined to be $M^2 X = 1.52$ and $M^2 Y = 1.36$. The data and fit curves are shown below in Figure 28.
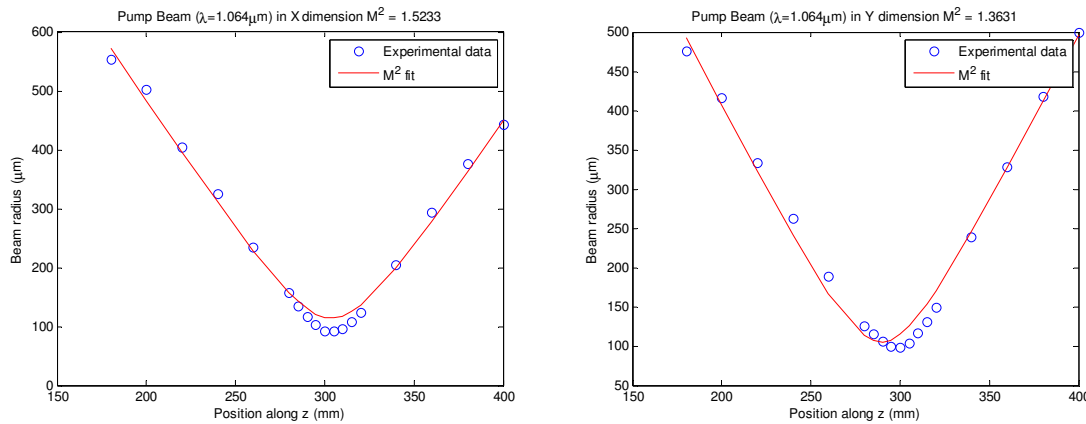
Figure 28: Fiber Amplifier Beam Profile with M² Waist Fit in X (left) and Y (right)

3.10 Fiber Amplifier Conclusions

This chapter explored many options in fiber amplifier design and provides a solution to the problems that occurred. As a result of these trials, certain "rules" regarding fiber amplifier design are easily established, where the figures and descriptions presented throughout this chapter demonstrate the origin of these "rules."

- End-caps should be spliced onto the active fiber

- Connectorization reduces environmental effects and protects the fiber

- Specialty optics to protect the pump laser are mandatory

- Spooling the fiber reduces higher-order modes at the cost of output power

- Careful mode-matching reduces higher-order modes without loss of power

- A camera connected to a video monitor can significantly aid alignment

- The pump side must be very carefully and cautiously aligned

Chapter 4
PPLN OPG

4.1 PPLN Setup and Alignment

Initially, the PPLN crystal used in this project was selected both because it was long, providing a much lower OPG threshold, and because it was a multi-grating crystal, offering many gratings to move to in the event that one did not activate. Visual inspection under the microscope also indicated a high poling quality of this sample. The crystal was measured to be 49mm long x 14mm wide x 1mm thick, and a Newport 561-TILT-LH five-axis stage (three transverse, tip/tilt, and rotate) was selected for sample positioning. A lens was needed to focus the fiber amplifier output into the crystal. The output of the fiber laser was profiled, and from this profile it is possible to obtain the Gaussian q-parameter. With the q-parameter we are then able to predict the effect of subsequent lenses on the beam size and hence we can choose a lens and lens position to optimally focus into the crystal. In the case of this PPLN crystal, the waist size needs to be less than 500 μm so as not to clip the beam profile.   Standard Gaussian beam propagation MATLAB code is reproduced in the appendix. A close-to optimal beam waist results in a Rayleigh range of ½ the crystal length.   (Equation 4), from which the beam waist was calculated, as shown below:

$$\text{Crystal Length} = 2z_R = 2\left(\frac{\pi w_0^2}{\lambda}\right)$$

$$49mm = \frac{2\pi w_0^2}{1.064\mu m}$$

$$w_0 = 91.1\mu m$$

The lens that produced a beam waist as close to the calculated waist as possible was f = 88.3 mm. The beam was then profiled after this lens so that the distance to the beam waist was known as well as the focused beam waist size, which was determined to be 85µm. A side-effect of the minor tweaking of the pump-side of the fiber amplifier meant that the output beam was not perfectly parallel to the table, so two mirrors were used after the focusing lens to create an axis at the height of the beam at the first mirror. Small base-plates were mounted to the five-axis stage to elevate the crystal to the newly defined beam axis. Shown in Figure 29 below is the final PPLN mounting stage setup. The simple stage is possible because heating the crystal was not necessary. In future work, placing the PPLN in an oven is advisable.
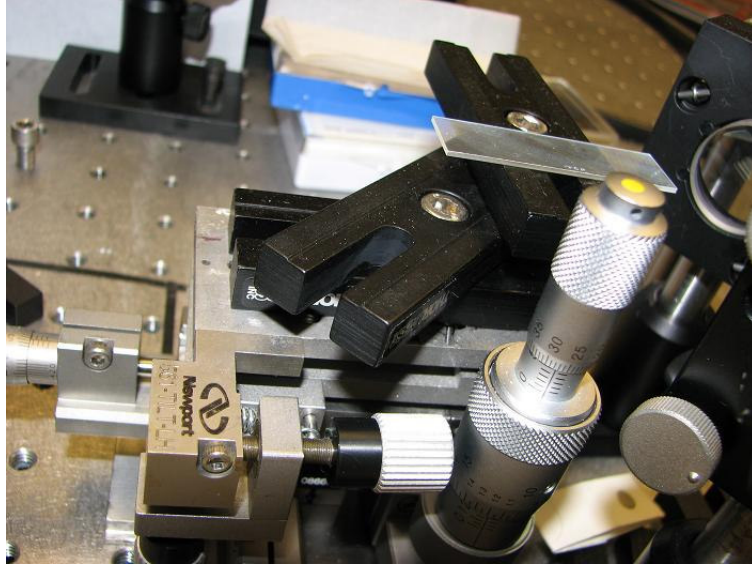
Figure 29: PPLN Multi-grating Crystal on Newport 5-Axis Stage

4.2 Polarization Control

The center of the crystal was placed at the beam waist and the stage was adjusted to maximize throughput. With the fiber amplifier fully pumped, there was a bright green output verifying that the fiber amplifier output was activating Second Harmonic Generation in the PPLN crystal, but there was no red beam (formed by Sum Frequency Generation of the pump and signal beams) to indicate the presence of the 1.5-µm OPG signal beam. This is not surprising since polarization is critical to the PPLN OPG device. The OPG process in PPLN requires that the pump be linearly polarized along the z-axis. A comment by Mr. Christopher Brooks from Aculight was remembered: there is no way to choose the alignment of stress rods in a connectorizer if there is a spliced end-cap. Where the in-house fiber was easily examined with a fiber microscope and adjusted to make the stress rods vertical, the fiber end-caps alter the image by

blurring the stress rods. Essentially, there was no known alignment in the fiber. It was then decided that two half-wave plates would be used, one before the seed laser couples into the fiber to rotate the seed beam to the fiber's alignment, and one before the PPLN focusing lens to rotate the fiber amplifier output beam to the crystal's vertical axis. Rotating the half-wave plates to visually maximize the red output (and thus the OPG signal beam), the green output was quickly matched in intensity by the red output, causing the final PPLN output beam to appear yellowish, as shown in Figure 30 below.
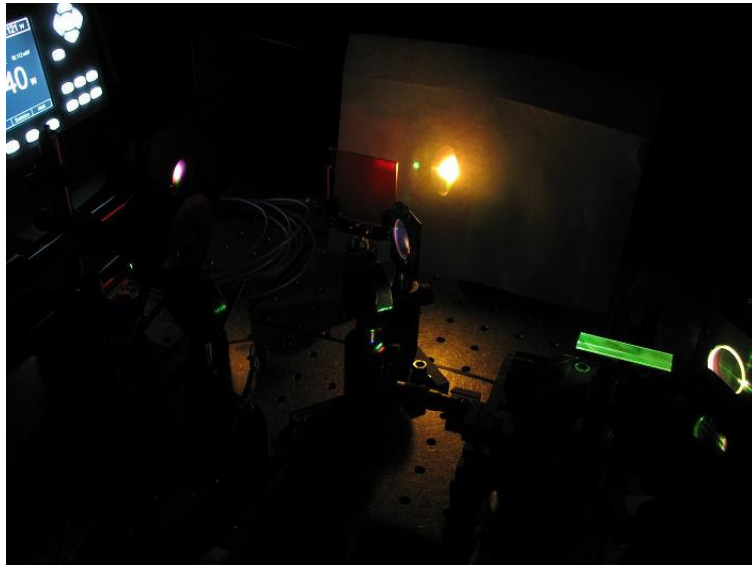

Figure 30: "Yellow" OPG Output

4.3   Filter Selection and Setup

The presence of multiple colors is a clear indication of OPG action. The red beam comes about via sum-frequency between the signal and the pump, hence if red is present copious signal is too. With the output spot showing

evidence of the signal beam, filters were selected to separate the signal beam from the rest of the PPLN output. Two filters that were recommended by Dr. Rita Peterson and Professor Lima, a germanium filter and an unknown filter that was approximately 0.75 mm thick, were tested using the Cary5000 to determine their transmittance at the pump wavelength, 1.064 µm, and at the signal wavelength, 1.5 µm. A third filter was also tested because it was reported to be highly transmissive at the pump wavelength and highly reflective at the signal wavelength. Transmission measurement results are shown below in Figure 31, with the three filters labeled "Ge" for the germanium filter, "Thin Filter" for the unknown filter, and "VLOC Dichroic" for the third filter tested.
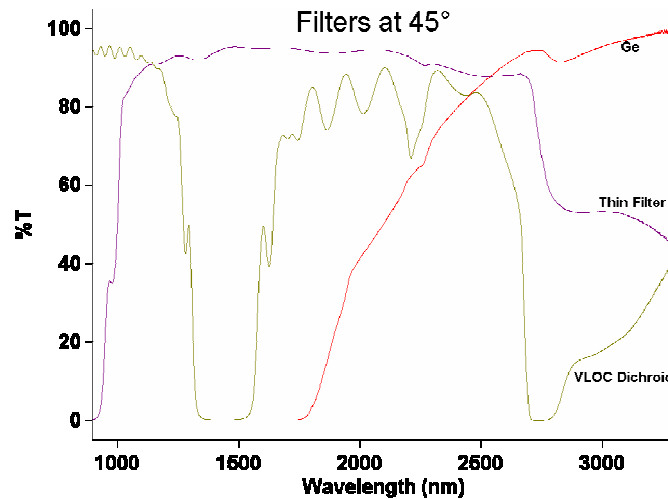
Figure 31: Filter Transmission Tests at 45°

From the above results, it was decided that the Ge filter would be used to separate out the majority of the idler beam and the dichroic would separate the signal from the pump. A diagram of the PPLN OPG setup is shown below in Figure 32.
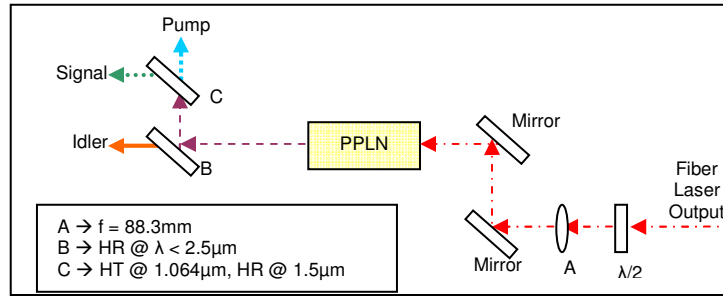
Figure 32: PPLN Crystal & OPG Filtering Setup Diagram

Of course, some of the green and red artifacts (and the other generated light) would still be combined with the signal beam, but these are typically considered weak overall, so they were ignored.

4.4 OPG Measurement and Results

A Newport 2935-C power meter was set up with two detector heads -- one for the signal and one for the idler -- so that the two beams could be measured simultaneously. Shown below in Figure 33 is the resulting power measurement with respect to fiber amplifier output power; shown in Figure 34 is the total conversion efficiency, defined as the signal plus idler powers divided by the incident pump power.
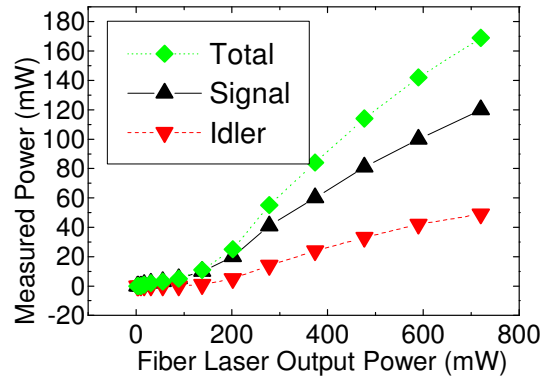
Figure 33: Total, Signal, and Idler Measured Power vs Pump Power
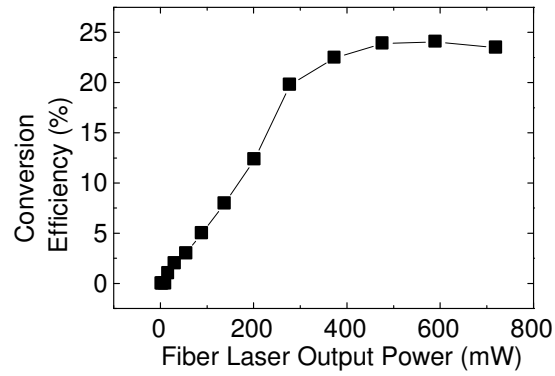
Figure 34: Total Conversion Efficiency vs Pump Power

At this point, the signal beam was guided to the SPEX Spectrometer and the final measurement graph, shown below in Figure 35, indicates a center wavelength of 1.508 µm with a bandwidth of 4 nm. Conservation of energy determines that the central idler wavelength is 3.613 µm.
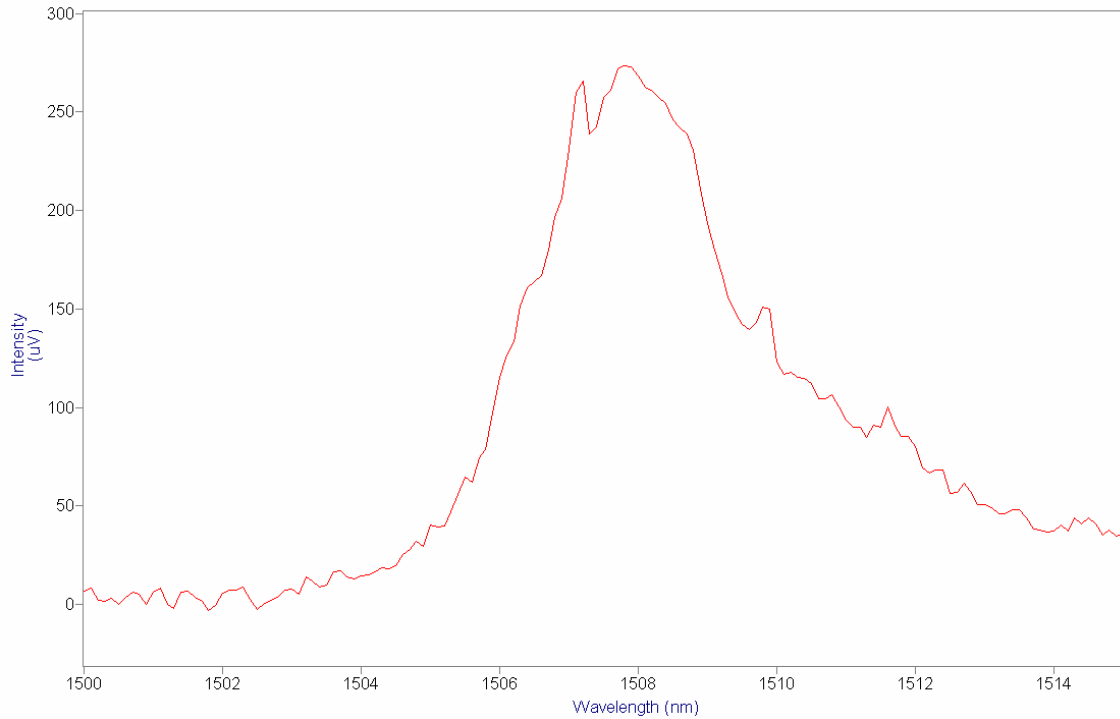
Figure 35: Signal Wavelength Spectrum

As previously mentioned, the PPLN crystal used was merely set in place and used to determine if OPG would occur, meaning that the grating period used had not been measured. The crystal position was recorded, along with the specific grating used, and the crystal was moved to a Nikon AZ100 microscope. Using the built-in software, calibrated in-house using a standard slide, dozens of measurement lines were drawn on the image (at maximum zoom) covering one, two, three, or four grating periods. The recorded image was magnified in order to determine which of the measurement lines were accurate; some of the lines were not accurate because of the limited resolution of the microscope display screen. All of the accurate measurements were recorded and averaged determining that the grating period used was 29.51 µm. Entering the pump wavelength, crystal material, and grating period into SNLO yielded an expected signal wavelength of

60

1.507 µm and an expected idler wavelength of 3.619 µm. This is consistent with the measured signal wavelength of 1.508 µm and the corresponding idler wavelength of 3.613 µm.

The signal beam was measured to have the same pulse width as the fiber amplifier, 0.5 ns; a pulse measurement is shown below in Figure 36.
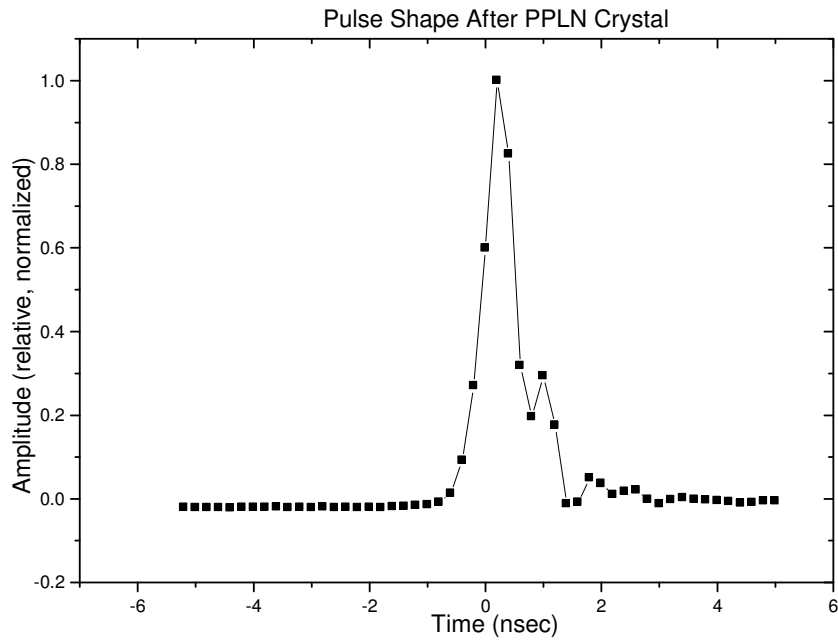
Figure 36: Signal Beam Pulse Shape

Chapter 5
Future Work

5.1   *Wavelength Division Multiplexers*

Wavelength Division Multiplexers (WDMs) are used to couple or decouple beams of different wavelengths and generally are comprised of a box with collimating lenses and dichroic mirrors firmly mounted in place, though the development of photonic band-gap structures indicates potential to become a single-unit WDM[42]. Shown in Figure 37 is a diagram of a WDM (left) and a photograph of a commercially available WDM (right) [43].

A: Dichroic mirror
B: Collimating Lens
C: Fiber
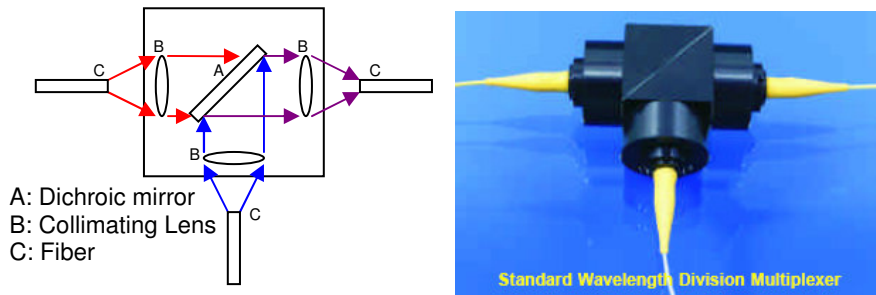
Figure 37: Wavelength Division Multiplexer Diagram and Photograph

Ideally, WDMs could benefit this project by removing all of the free-space optics that are used to guide and couple the pump and seed beams into the fiber. Figure 38 shows a diagram of the project design with connectorized WDMs replacing the dichroic mirrors and free space options used in this project.

62
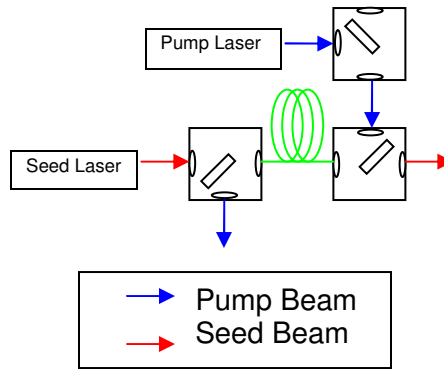
Figure 38: Fiber Amplifier Design with WDMs

During this project, the WDM option was explored by contacting OzOptics, though no product matching this project was available at that time.

5.2   OPG-Seeded Fiber

One improvement to the OPG is to seed the OPG with a monochromatic laser tuned within the signal bandwidth of the OPG (~1500 nm in this work) to narrow the signal spectrum. This has been done before[44,45] by aligning a seed laser to the input of the nonlinear crystal. However, coupling the seed laser into the active fiber ensures that the OPG seed laser will be aligned to the nonlinear crystal without additional optics. Because the fiber is highly multimode at 1064 nm, it turns out that it is still able to guide 1550 nm. According to equations 1 and 2 approximately 25 modes will guide. Fortunately, mode-filtering will occur for the 1550 nm as does for the 1064 nm due to the spooling. When coupling the OPG seed laser into the fiber, two considerations to make are that additional filtering optics will be necessary to protect the various lasers and that the half-

wave plates used to rotate the polarization of the fiber amplifier seed beam will affect the polarization of the OPG seed laser. The additional dichroics necessary to protect the lasers will reduce the coupling efficiency of the lasers and therefore the maximum fiber amplifier output power, but proof that the seeded fiber concept reduces the signal beam bandwidth is the goal.

5.3   Photonic Crystal Fiber

An option for improving the beam quality of the fiber amplifier without the need to spool the fiber is by using a Photonic Crystal Fiber. Available commercially doped with ytterbium[46], Photonic Crystal Fibers have shown both single mode propagation over a wide range of wavelengths[47] and polarization maintaining capability[48].

5.4   Enhanced Optical Filtering

One aspect of this experiment that was not optimized was the optical filtering of the PPLN output. A better filtering scheme could be arranged that would completely separate the signal beam from the pump and idler beams, as well as the SHG green and SFG red beams (and the other associated artifacts).

The simplest way to do this is to use dichroic mirrors that reflect one wavelength while transmitting the others. For example, a 1064 HR with a 1550

and 3390 HT followed by a 1550 HR and 3390 HT will result in three outputs for the pump signal and idler. The advantage of this scheme is none of the energy of the pump signal or idler are lost.

Appendices

Appendix One: ASSP Paper

The following paper was prepared for and submitted to the Optical Society of America's Advanced Solid-State Photonics conference to be held January 27-30, 2008, in Nara, Japan. The paper was approved for a poster presentation on January 30, 2008.

Sub-nanosecond infrared optical parametric pulse generation in PPLN pumped by a seeded fiber amplifier

Matthew D. Cocuzzi and Kenneth L. Schepler
Air Force Research Lab, Wright Patterson Air Force Base
2241 Avionics Circle, WPAFB, OH 45433-7304
Phone: (937) 904-9667
Fax: (937) 656-5512
Email: matthew.cocuzzi@wpafb.af.mil

Peter E. Powers
Department of Physics and the Electro-Optics Program, University of Dayton, 300 College Park, Dayton, OH 45469-2314

Ivan T. Lima, Jr.
Department of Electrical and Computer Engineering, North Dakota State University, Fargo ND 58105

Abstract: Sub-nanosecond pulses generated in a microchip laser were amplified in an Yb-doped, polarization-maintaining fiber amplifier and converted with 24% efficiency to infrared wavelengths using a periodically poled lithium niobate optical parametric generator.

1. Introduction

Optical parametric generators (OPG) based on periodically poled lithium niobate (PPLN) have been well characterized in recent years, largely as a result of the high nonlinearity (d_{33} = 27pm/V) [1], noncritical phasematching and simple fabrication of PPLN. Efficient operation in the nanosecond and femtosecond regime is possible when pumped by high-peak-power pulsed lasers. [2-4] Continued development of the polarization maintaining fiber needed for nonlinear interactions has led to fiber laser pumped PPLN frequency conversion devices. Erbium [5, 6] and ytterbium fiber lasers [7, 8] have been used to pump PPLN and generate tunable mid-infrared output.

In this paper we report efficient generation of sub-nanosecond pulses in the mid-IR spectral region using optical parametric generation in a PPLN crystal pumped by 1064-nm pulses from an Yb-doped fiber amplifier. The fiber amplifier was seeded with 0.5-ns pulses.

2. Experiment

The fiber laser system, used as our OPG pump, was built as shown in Figure 1. The seed laser was a Teem Photonics Nd:YAG microchip laser operating at 1064 nm, polarized 99:1, 7.14-kHz repetition rate, 0.5-nsec pulse width, average power of 38 mW, and 5.3 µJ pulse energy. The fiber amplifier was pumped at 915 nm using an EM4, Inc. diode laser. The diode laser was coupled to a fiber pigtail and operated at a maximum of 6 W with 7 A of operating current. An Yb^{3+}-doped, panda-structure, polarization-maintaining (PM), double-clad fiber manufactured by Liekki was the active element and had a 25-µm core diameter and a 248-µm inner cladding diameter. The fiber was 3.56 m long and FC connectorized; 400-µm diameter silica end-caps were spliced to it to prevent damage and polished at 8° to normal to prevent back reflections. A pair of dichroic mirrors with 98% transmission at 1064 nm and 98% reflection at 915 nm (both measurements for 45° incidence) coupled the pump beam into the fiber and isolated the pump laser from damage by 1064-nm pulses. A second pair of dichroic mirrors blocked pump light from reaching the seed laser. An isolator was used to prevent back-reflections of 1064-nm light into the seed laser. A half-wave plate was used to rotate the seed beam polarization to match it to the PM axis of the fiber.

Knife-edge beam profiling was utilized to mode-match both the pump and seed beams into the fiber. The seed beam coupling efficiency was 55% and the pump beam coupling efficiency was 96%. The fiber output pulse width was 0.5 ns, the same as the input seed laser pulse width. Because the fiber core did not limit the beam to single transverse mode propagation, we coiled the fiber in 7.5-cm diameter loops to inhibit higher order modes. [9] The average output power of the fiber amplifier with respect to the average power of the diode

pump laser is shown in Figure 2; a maximum output power of 720 mW was achieved at 6 W of pump power and 20 mW of seed power coupled into the fiber.
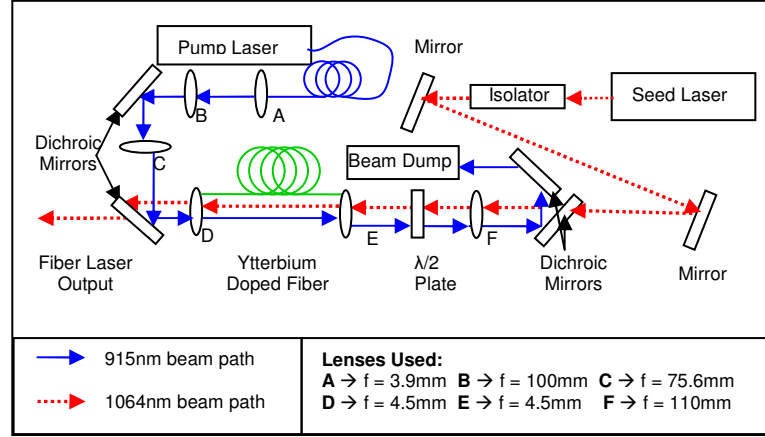
Figure 1: Fiber Laser Setup – Microchip seed laser pulses at 1064 nm are amplified in an ytterbium-doped, polarization maintaining fiber. The fiber amplifier is pumped by a 915-nm diode laser.
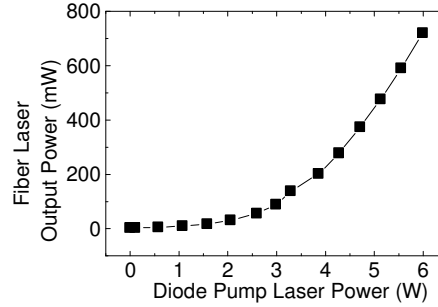
Figure 2: Fiber amplifier output power vs. diode laser pump power.

The output of the fiber laser was focused to a beam waist of 88 µm. A PPLN crystal was mounted on a 5-axis stage (3 translation, rotation, tilt) in a position such that the beam waist was at the center of the crystal. The PPLN crystal was a 1-mm x 14-mm cross-section x 49-mm long multi-grating crystal with no coatings and approximate parallelism of the front and back surfaces. The domain grating period used was 29.5 µm, which corresponds to expected 1.507-µm signal and 3.619-µm idler wavelengths based upon $LiNbO_3$ Sellmeier equations. A half-wave plate was used to rotate the fiber laser output polarization to align with the z-axis in the PPLN crystal, hence maximizing the OPG output. The PPLN output was separated by two filters to isolate the signal and idler as shown in the diagram of the setup below (Figure 3).

The PPLN OPG output was separated and the signal and idler beams measured simultaneously. Figure 4 shows the average power of the signal and idler beams (and total power) with respect to fiber laser output power. A combined signal and idler average power of 170 mW (120 mW for signal alone) was achieved with 720 mW of 1064-nm input power. This corresponds to 17 µJ/pulse and 34 kW peak power for the signal pulses. Optical-to-optical conversion efficiency was 24%. Figure 5 shows the conversion efficiencies of the signal and idler beams (and total efficiency) with respect to fiber laser output power.
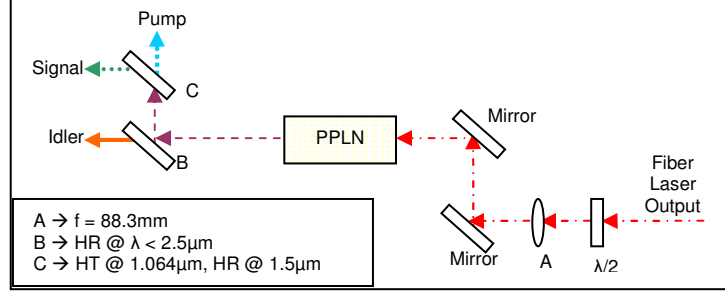
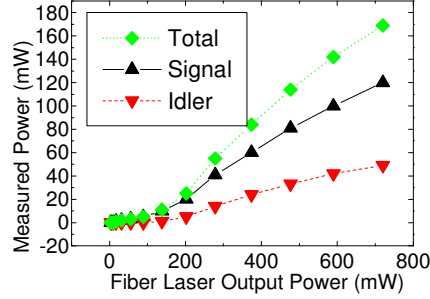**Figure 3: OPG Configuration – Fiber Laser Pumped PPLN and Output Filtering.**

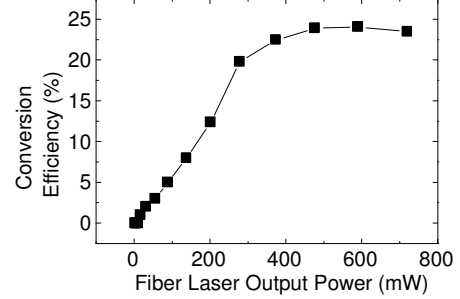**Figure 4: Signal, Idler, and Total Output Power of the PPLN OPG.**

Figure 5: Total OPG Conversion Efficiency.

The signal beam was measured to have a center wavelength of 1.508 µm (reasonably close to the predicted 1.507 µm) and a bandwidth of 3.6 nm. Conservation of energy dictates a calculated idler wavelength of 3.61 µm.

3. Conclusions:

We have demonstrated 24% conversion efficiency of sub-nanosecond pulses using OPG in a PPLN crystal. A polarization-maintaining Yb fiber amplifier generated 720 mW of average pump power from 20 mW of injected pulses produced by a microchip laser. The relatively large 3.6-nm bandwidth and the beam quality could be further improved with seeding of the OPG, a step OPG we plan to implement soon. The device was stable and simple to align. It could be easily packaged into a rugged and device ideal for generation of high repetition rate, sub-nanosecond pulses. Such pulse formats are ideal for eye-safe, high-resolution laser ranging.

References:

[1] L. E. Myers, R. C. Eckardt, M. M. Fejer, R. L. Byer, W. R. Bosenberg, and J. W. Pierce, "Quasi-phase-matched optical parametric oscillators in bulk periodically poled LiNbO₃," *Journal of the Optical Society of America B*, **12**, pp. 2102-2116, 1995.

[2] U. Baeder, J.-P. Meyn, J. Bartschke, T. Weber, A. Borsutzky, R. Wallenstein, R. G. Batchko, M. M. Fejer, and R. L. Byer, "Nanosecond periodically poled lithium niobate optical parametric generator pumped at 532 nm by a single-frequency passively Q-switched Nd:YAG laser," *Optics Letters*, **24**, pp. 1608-1610, 1999.

[3] J. J. Zayhowski, "Periodically poled lithium niobate optical parametric amplifiers pumped by high-power passively Q-switched microchip lasers," *Optics Letters*, **22**, pp. 169-171, 1997.

[4] B.-G. Zhang, J.-Q. Yao, X. Ding, H. Zhang, P. Wang, D.-G. Xu, G.-J. Yu, and F. Zhang, "Low-threshold, high-efficiency, high-repetition-rate optical parametric generator based on periodically poled LiNbO₃," *Chinese Physics*, **13**, pp. 364-368, 2004.

[5] P. E. Britton, H. L. Offerhaus, D. J. Richardson, P. G. R. Smith, G. W. Ross, and D. C. Hanna, "Parametric oscillator directly pumped by a1.55-mm erbium-fiber laser," *Optics Letters*, **24**, pp. 975-977, 1999.

[6] A. Galvanauskas, M. A. Arbore, M. M. Fejer, M. E. Fermann, and D. J. Harter, "Fiber-laser-based femtosecond parametric generator in bulk periodically poled LiNbO₃," *Optics Letters*, **22**, pp. 105-107, 1997.

[7] R. Paschotta, J. Nilsson, A. C. Tropper, and D. C. Hanna, "Ytterbium-doped fiber amplifiers," *IEEE Journal of Quantum Electronics*, **33**, pp. 1049-1056, 1997.

[8] H. M. Pask, R. J. Carman, D. C. Hanna, A. C. Tropper, C. J. Mackechnie, P. R. Barber, and J. M. Dawes, "Ytterbium-doped silica fiber lasers: versatile sources for the 1-1.2 mm region," *IEEE Journal of Quantum Electronics*, **1**, pp. 2-13, 1995.

[9] J. P. Koplow, D. A. V. Kliner, and L. Goldberg, "Single-mode operation of a coiled multimode fiber amplifier," *Optics Letters*, **25**, pp. 442-444, 2000.

Appendix Two: MATLAB Code

Note: the MATLAB color and font scheme has been preserved. The final listing is one that is referenced in some of the following files but is not referenced in the Text of this thesis. Additionally, it is understood that the distance terms in the pump-laser-coupling sections is somewhat confusing. Shown below is a rough diagram of the system and the distances to which MATLAB refers.
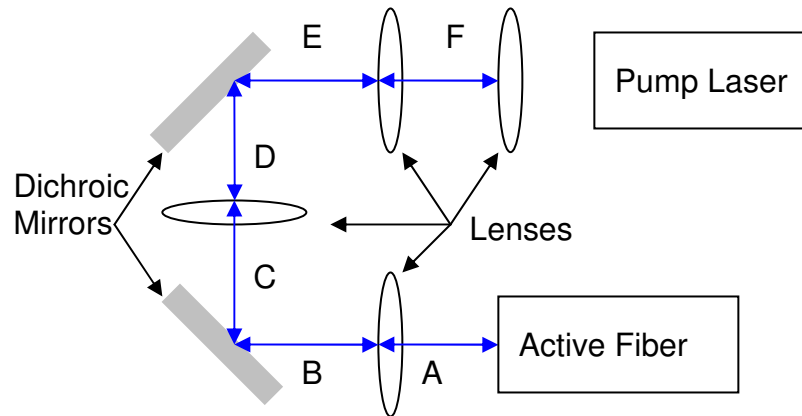
Figure 39: Diagram of Pump Coupling Distances

Listing 1: distance.m

```
function q = distance(q,d)
%%% This function takes the q-parameter "q" and
%%% propagates it through a distance "d" (meters)
%%% and returns the new "q"
A = 1;
B = d;
C = 0;
D = 1;

q = (A*q+B)./(C*q+D);
```

Listing 2: lens.m

```
function q = lens(q,f)
%%% This function takes the q-parameter "q" and
%%% propagates it through a thin lens of focal
%%% length "f" (meters) and returns the new "q"
A = 1;
B = 0;
C = -1/f;
D = 1;

q = (A*q+B)./(C*q+D);
```

Listing 3: qwaist.m

```
function q = qwaist(w,lambda)
%%% This function takes a desired or known beam waist "w"
%%% and a known wavelength "lambda," and returns the
%%% q-parameter "q" for that beam waist
zr = pi*w.^2/lambda;
qinv = -j./zr;

q = 1./qinv;
```

Listing 4: omega.m

```
function w = omega(q,lambda)
%%% This function takes the q-parameter "q" and the wavelength
%%% "lambda," passed at the function call, and determines
%%% the beam waist (radius).
qx = 1./q;
w = sqrt(lambda./(-imag(qx)*pi));
```

Listing 5: M2calc.m

```
function E = M2calc(x)
%%% This function was written by Jim Alverson to
%%% determine the M^2 of a beam based on a set of
%%% data points to which an M^2-modified Gaussian
%%% Beam Waist equation is fit.
```

```
W0 = x(1);        M = x(2);        z0 = x(3);
load fitdata
E1 = W.^2 - (W0.^2 + M.^4.*(lambda.^2./(pi.^2.*W0.^2).*(z-z0).^2));
E1 = sqrt(sum((1e9.*E1).^2)) + (M < 1) .* (1-M) .* 1e25 + ...
        (z0 < 0) .* abs(z0) .* 1e25 + (W0 < 0) .* abs(W0) .* 1e25;
E = E1;
```

Listing 6: missingL.m

```
function L = missingL(Lp,Ls,Li);
%%% This function takes two wavelengths (or two vectors
%%% of wavelengths) and determines what the resulting
%%% wavelength would be from a nonlinear interaction.
%%% When the function is passed, the unknown wavelength
%%% is passed as zero.
if (Lp == 0)
    Lp = (1./Ls + 1./Li).^-1;
    L = Lp;
end
if (Ls == 0)
    Ls = (1./Lp - 1./Li).^-1;
    L = Ls;
end
if (Li == 0)
    Li = (1./Lp - 1./Ls).^-1;
    L = Li;
end
```

Listing 7: pump_beam_coupling_setup.m

```
clc;clear all;%close all;
%%% This is the final configuration of the pump beam
%%% coupling into the fiber

%%% Starting assumptions
dwaist = 1e-4; %desired beam waist at the fiber
mwaist = 2.5e-6; %measured beam waist at the fiber
Da = 1.8e-3;
L = 915e-9; %wavelength in meters
% the lenses available in the lab:
ffocus = [75.6 88.3 100 150 175 200 250 500 1000];
ffocuss = ffocus*1e-3; %converting to (mm)
fcoll = 4.5e-3; %fiber focusing lens
np = 501; %number of points for calculations
DA = 4.5272e-3; %distance from waist to fiber lens
DB = 5.5e-2 - 2.54e-3; %distance from fiber lens to Mirror1
DC = 4e-2; %distance from Mirror1 to path focusing lens
DD = 5e-2; %distance from path focusing lens to Mirror2
DE = 15e-2; %distance from Mirror2 to pump collimating lens

D1 = DA;
Doff = linspace(-.04,.20,24);
D2 = DB+DC-.05;
D3 = DD+DE+.05;
```

```matlab
F = ffocuss(3); %selecting 2 lenses to use
F2 = ffocuss(2);

%propagating the measured beam back to the pump lens
q0 = qwaist(mwaist,L);
q1 = distance(q0,DA);
q2 = lens(q1,fcoll);
q3 = distance(q2,D2);
q4 = lens(q3,F);
q5 = distance(q4,D3);

%defining distances for plotting purposes
D1x = linspace(0,D1,np);
Dax = linspace(0,Da,np);
D2x = linspace(0,D2,np);
D3x = linspace(0,D3,np);
D3a = .32*D3;
DDD1 = linspace(0,D3a,np);
DDD2 = linspace(D3a,D3,np);


%%%
%q5 = 0.1895 + 0.0172i;
%%%

%%% START
%claculations for all 3 systems: see the legend at the end
%note that the "distances" and "lenses" encoutered are
%not the same for each of the three systems because one
%is not being calculated in the same direction as the others
q0 = qwaist(dwaist,L);
%%% FIRST DISTANCE
for a = 1:np
    %note that back-calculations have negative values
    %in their function calls
    q1 = distance(q0,-D1x(a));
    w1(a) = omega(q1,L);
    qm1 = distance(q5,D3x(a));
    wm1(a) = omega(qm1,L);
    qx1 = distance(q5,DDD1(a));
    wx1(a) = omega(qx1,L);
end
%FIRST LENS
q2 = lens(q1,-fcoll);
qm2 = lens(qm1,F);
qx2 = lens(qx1,F2);
%SECOND DISTANCE
for b = 1:np
    q3 = distance(q2,-D2x(b));
    w3(b) = omega(q3,L);
    qm3 = distance(qm2,D2x(b));
    wm3(b) = omega(qm3,L);
    qx3 = distance(qx2,DDD1(b));
    wx3(b) = omega(qx3,L);
end
%SECOND LENS
q4 = lens(q3,-F);
qm4 = lens(qm3,fcoll);
```

```
qx4 = lens(qx3,F);
%THIRD DISTANCE
for c = 1:np
    q5 = distance(q4,-D3x(c));
    w5(c) = omega(q5,L);
    qm5 = distance(qm4,D1x(c));
    wm5(c) = omega(qm5,L);
    qx5 = distance(qx4,D2x(c));
    wx5(c) = omega(qx5,L);
end
%THIRD LENS
%the only system that sees three lenses is the newly
%calculated system to fit the known starting point and
%the desired ending point
qx6 = lens(qx5,fcoll);
%FOURTH DISTANCE
for d = 1:np
    qx7 = distance(qx6,D1x(d));
    wx7(d) = omega(qx7,L);
end
%defining arrays of distances/beam waists for plotting
Z1 = [-D1x -D2x-D1 -D3x-D1-D2] + .297;
Z2 = [D3x D2x+D3 D1x+D2+D3];
W = [w1 w3 w5];
WM = [wm1 wm3 wm5];
WX = [wx1 wx3 wx5 wx7];
ZX = [DDD1 DDD2 D2x+D3 D1x+D2+D3];

figure(1)
plot(Z1,W*1e3,'b',Z2,WM*1e3,'k--',ZX,WX*1e3,'r:')
xlabel('position (relative) (m)')
ylabel('beam radius (mm)')
stra = 'Target Beam';
strb = 'Actual Beam';
strc = 'Solution Beam';
legend(stra,strb,strc)
title('Beam Profile Back Calculations')
grid on
```

Listing 8: pump_beam_final_coupling.m

```
clc;clear all;%close all;
%%% This is the final copy of the program used to show
%%% exactly what happens to the pump beam as it couples
%%% into the fiber. Note that the legacy code (the FOR
%%% loop, the options of distances/lenses/etc) was
%%% originally used to show three options at a time,
%%% including the absolutely ideal coupling
%plot(0,0,'k')
hold on
%Setting up the initial conditions
wo = 1e-3; %beam waist
np = 501; %number of points
L = 915e-9; %wavelength
LenS = [250e-3 62.9e-3 50.2e-3]; %lenses
```

```
lens2 = 4.5e-3;
%lens_location = (24 + 5.64 - lens1*100);
%FF = linspace(22.15e-2,22.3e-2,5);
color = ['k' 'r' 'b'];
%for ab = 1:3
ab = 3;
lens1 = LenS(ab);
%distances for the upcoming calculations
FF = [4.64e-2 22.85e-2 24.1e-2];
F = FF(ab);%FF(ab);%22.25e-2;
CDE = 24e-2 - F;
B = 5.64e-2;
A = 10*(3.555+1.2)*1e-3;

%propagation calculations
%reminder: plotw(q-parameter,distance,point,wavelength)
q0 = qwaist(wo,L);
[wq1 q1] = plotw(q0,F,np,L);
q2 = lens(q1,lens1);
[wq2 q3] = plotw(q2,CDE+B,np,L);
q4 = lens(q3,lens2);
[wq3 q5] = plotw(q4,A,np,L);

%setting up plot points/locations
plot_dist = pdst(np,F,CDE+B,A);
w = [wq1(1,:) wq2(1,:) wq3(1,:)];
%pause
plot(plot_dist*1e3,w*1e6,color(ab))
axis([.28*1e3 .32*1e3 0 12e-5*1e6])
%end
hold off
grid on
xlabel('Position in Pump Beam Path (mm)')
ylabel('Beam Radius (µm)')
title('Beam Radius Along Pump Beam Path')
hold on
plot(296.4,104,'ro') %this is the pump coulping lens
hold off
%hold on
%text(297,105,'\leftarrow Pump Coupling Lens Location')
%hold off
legend('beam radius','pump coupling lens')
```

Listing 9: BeamFit21Sept07.m

Note: This file requires data generated in the next listing, [M10]

```
close all
%%% This file was written initially by Jim Alverson to
%%% coincide with the M2Fit function. Modifications were
%%% made as data was collected -- the changes are noted

% x = x/2;
%%% The NanoScan numbers were 1.3562 times smaller than
```

```matlab
%%% manual knife-edge data at the same location. Below
%%% are the adjustments for both the 1.3562 factor and
%%% a halving due to the fact that the NanoScan data
%%% are measurements of the diameter
x = qq(:,3)*1.3562/2;
% y=y/2;
y = qq(:,5)*1.3562/2;
z = qq(:,1)/1000;
lambda = 1.064e-6;
%initial guesses for [w0, M, z0] -- these need to be close!
%recommended: run the program once, then adapt these numbers
V0 = [1.4e-4 1.2 0.33];
W = x;
save fitdata W z lambda
[V] = fminsearch(@M2calc,V0,optimset('MaxIter',1e9,'TolFun',1e-6));
Vpx = V

figure; plot(1e3*z,1e6*W,'bo');
hold on;
plot(1e3*z,1e6*sqrt((V(1).^2 +
V(2).^4.*(lambda.^2./(pi.^2.*V(1).^2)).*(z-V(3)).^2)),'r');
xlabel('Position along z (mm)');
ylabel('Beam radius (\mum)');
title(['Pump Beam (\lambda=1.064\mum) in X dimension M^2 = '
num2str(Vpx(2).^2) ]);%(W0 = ' ...
%    num2str(Vpx(1)*1e3) 'mm, M^2 = ' num2str(Vpx(2).^2) ', z0 = '
num2str(Vpx(3)*1e3) 'mm)']);
legend('Experimental data','M^2 fit');


W = y;
save fitdata W z lambda
[V] = fminsearch(@M2calc,V0,optimset('MaxIter',1e9,'TolFun',1e-6));
Vpy = V

figure; plot(1e3*z,1e6*W,'bo');
hold on;
plot(1e3*z,1e6*sqrt((V(1).^2 +
V(2).^4.*(lambda.^2./(pi.^2.*V(1).^2)).*(z-V(3)).^2)),'r');
xlabel('Position along z (mm)');
ylabel('Beam radius (\mum)');
title(['Pump Beam (\lambda=1.064\mum) in Y dimension M^2 = '
num2str(Vpy(2).^2) ]);% (W0 = ' ...
  %  num2str(Vpy(1)*1e3) 'mm, M^2 = ' num2str(Vpy(2).^2) ', z0 = '
num2str(Vpy(3)*1e3) 'mm)']);
legend('Experimental data','M^2 fit');


%        %%        %
%     %        %       %
%%% SIGNAL SECTION %%%
%     %        %       %
%        %%        %
%z = qqq(:,1)/1000;
%x = qqq(:,2).*1e-6*1.3562/2;
%y = qqq(:,3).*1e-6*1.3562/2;
z = Ap; x = (Ax8-Ax92); y = (Ay8-Ay92);
```

```matlab
lambda = 1.507e-6;
%initial guesses for [w0, M, z0] as before
V0 = [25e-6 2 22e-3];
W = x;

save fitdata W z lambda
[V] = fminsearch(@M2calc,V0,optimset('MaxIter',1e9,'TolFun',1e-6));
Vsx = V

figure; plot(1e3*z,1e6*W,'bo');
hold on;
plot(1e3*z,1e6*sqrt((V(1).^2 +
V(2).^4.*(lambda.^2./(pi.^2.*V(1).^2)).*(z-V(3)).^2)),'r');
xlabel('Position along z (mm)');
ylabel('Beam radius (\mum)');
title(['Signal Beam (\lambda=1.507\mum) in X dimension M^2 = '
num2str(Vsx(2).^2) ]);% (W0 = ' ...
    %num2str(Vsx(1)*1e3) 'mm, M^2 = ' num2str(Vsx(2).^2) ', z0 = '
num2str(Vsx(3)*1e3) 'mm)']);
legend('Experimental data','M^2 fit');

W = y;
z = Ap2;
V0 = [25e-6 2 22e3];
save fitdata W z lambda
[V] = fminsearch(@M2calc,V0,optimset('MaxIter',1e9,'TolFun',1e-6));
Vsy = V

figure; plot(1e3*z,1e6*W,'bo');
hold on;
plot(1e3*z,1e6*sqrt((V(1).^2 +
V(2).^4.*(lambda.^2./(pi.^2.*V(1).^2)).*(z-V(3)).^2)),'r');
xlabel('Position along z (mm)');
ylabel('Beam radius (\mum)');
title(['Signal Beam (\lambda=1.507\mum) in Y dimension M^2 = '
num2str(Vsy(2).^2) ]);% (W0 = ' ...
    %num2str(Vsy(1)*1e3) 'mm, M^2 = ' num2str(Vsy(2).^2) ', z0 = '
num2str(Vsy(3)*1e3) 'mm)']);
legend('Experimental data','M^2 fit');
```

Listing 10: beam_data_sept_24.m

```matlab
%clc;clear all;close all;
%%% This is the collection of data obtained for
%%% M^2 calculations. The PUMP DATA was gathered
%%% with the NanoScan, and the SIGNAL DATA was
%%% gathered using a knife-edge profile. Both
%%% were modified and plotted in a different
%%% MATLAB file (BeamFit21Sept07.m)

% % % PUMP DATA % % %
% % September 24th % %
% structure: [position,X(µm),X(m),Y(µm),Y(m)]
```

```
qq=[180 817 8.17E-4 701 7.01E-4
200 742 7.42E-4 615 6.15E-4
220 597 5.97E-4 491 4.91E-4
240 479 4.79E-4 388 3.88E-4
260 346 3.46E-4 278 2.78E-4
280 232 2.32E-4 186 1.86E-4
285 199 1.99E-4 170 1.7E-4
290 173 1.73E-4 156 1.56E-4
295 151 1.51E-4 146 1.46E-4
%296    146 1.46E-4 144 1.44E-4
%297    142 1.42E-4 143 1.43E-4
%298    139 1.39E-4 142 1.42E-4
300 135 1.35E-4 145 1.45E-4
%301    132 1.32E-4 144 1.44E-4
%302    134 1.34E-4 148 1.48E-4
%303    136 1.36E-4 156 1.56E-4
305 135 1.35E-4 153 1.53E-4
310 140 1.4E-4  171 1.71E-4
315 158 1.58E-4 193 1.93E-4
320 182 1.82E-4 221 2.21E-4
340 302 3.02E-4 353 3.53E-4
360 434 4.34E-4 484 4.84E-4
380 554 5.54E-4 616 6.16E-4
400 653 6.53E-4 736 7.36E-4];

% % % SIGNAL DATA % % %
% % September 25th % %
qqq = [200  156 166
201 144 155
202 132 144
203 120 131
204 104 119
205 99  107
206 86  95
207 75  84
208 66  77
209 57  71
210 51  62
211 43  55
212 40  48
213 41  53
214 41  56
215 46  70
216 54  78
217 62  88
218 75  100
219 87  113
220 98  121];

%%% NOVEMBER 5th %%%
% Y AXIS %
p = [.2:.1:1.9];
y92a1 = [6973 6980 6971 6971 6970 6967 6966 6960];
y92a2 = [6966 6955 6939 6932 6920 6916 6895 6877 6881 6855];
y92a = [y92a1 y92a2];
y8a1 = [7177 7153 7130 7090 7070 7040 7017 6991];
y8a2 = [7000 7007 7020 7040 7055 7075 7088 7109 7129 7145];
```

```
y8a = [y8a1 y8a2];

y92 = .1*y92a/2000;
y8 = .1*y8a/2000;
Ap2 = p*2.54/100;
Ay92 = y92*2.54/100;
Ay8 = y8*2.54/100;

% X AXIS %
p = [.2:.1:1.6];
x92a1 = [6960 6972 6997 7024 7052 7077 7092 7112];
x92a2 = [7375 7392 7415 7431 7446 7465 7487];
x92a = [x92a1 x92a2];
x8a1 = [7121 7125 7125 7130 7131 7131 7130 7138];
x8a2 = [7397 7439 7470 7508 7544 7582 7619];
x8a = [x8a1 x8a2];

x92 = .1*x92a/2000;
x8 = .1*x8a/2000;
Ap = p*2.54/100;
Ax92 = x92*2.54/100;
Ax8 = x8*2.54/100;
```

Listing 11: plotw.m

```
function [w q] = plotw(q,dist,points,lambda)
%%% This function propagates a Gaussian beam's q-parameter
%%% over a distance "dist," for a "points" number of points,
%%% at wavelength "lambda." The result of the function is
%%% that the beam waist is calculated at every position so
%%% that it can be easily plotted and the final q-parameter
%%% is determined and ready for use in the next calculation.
d = linspace(0,dist,points);
for a = 1:points
    q1 = distance(q,d(a));
    w(1,a) = omega(q1,lambda);
end
q = q1;
```

References

1. L. E. Myers, R. C. Eckardt, M. M. Fejer, R. L. Byer, W. R. Bosenberg, and J. W. Pierce, "Quasi-phase-matched optical parametric oscillators in bulk periodically poled LiNbO3," *J. Opt. Soc. Am. B* **12** (1995)

2. J. J. Zayhowski, "Periodically poled lithium niobate optical parametric amplifiers pumped by high-power passively *Q*-switched microchip lasers," *Opt. Lett.* **22** (1997)

3. U. Bäder, J. P. Meyn, J. Bartschke, T. Weber, A. Borsutzky, R. Wallenstein, R. G. Batchko, M. M. Fejer, and R. L. Byer, "Nanosecond periodically poled lithium niobate optical parametric generator pumped at 532nm by a single-frequency passively Q-switched Nd:YAG laser," *Opt. Lett.* **24** (1999)

4. Zhang Bai-Gang, Yao Jian-Quan, Ding Xin, Zhang Hao, Wang Peng, Xu De-Gang, Yu Guo-Jun, Zhang Fan, "Low-threshold, high-efficiency, high-repetition-rate optical parametric generator based on periodically poled LiNbO3," *Chinese Phys.* **13** (2004)

5. A. Galvanauskas, M. A. Arbore, M. M. Fejer, M. E. Fermann, and D. Harter, "Fiber-laser-based femtosecond parametric generator in bulk periodically poled LiNbO3," *Optics Letters* **22** (1997)

6. P. E. Britton, H. L. Offerhaus, D. J. Richardson, P. G. R. Smith, G. W. Ross, and D. C. Hanna, "Parametric oscillator directly pumped by 1.55um erbium-fiber laser," Opt. Lett. **24** (1999)

7. Pask, H.M.; Carman, R.J.; Hanna, D.C.; Tropper, A.C.; Mackechnie, C.J.; Barber, P.R.; Dawes, J.M., "Ytterbium-doped silica fiber lasers: versatile sources for the 1-1.2 µm region," *IEEE Journal of Selected Topics in Quantum Electronics* **1** (1995)

8. Paschotta, R.; Nilsson, J.; Tropper, A.C.; Hanna, D.C., "Ytterbium-doped fiber amplifiers," *IEEE Journal of Quantum Electronics* **33** (1997)

9. J. P. Koplow, D. A. V. Kliner, L. Goldberg, "Single-mode operation of a coiled multimode fiber amplifier," *Opt. Lett.* **25** (2000)

10. http://www.laser2000.co.uk/ds/DS_00277.pdf

11. R.J. Mears, L. Reekie, I.M. Jauncey and D.N. Payne: "Low-noise Erbium-doped fibre amplifier at 1.54pm," *Electron. Lett.* **23** (1987)

12. E. Desurvire, J. Simpson, and P.C. Becker, "High-gain erbium-doped traveling-wave fiber amplifier," *Optics Letters* **12** (1987)

13. J. Limpert, A. Liem, T. Gabler, H. Zellmer, and A. Tünnermann, "High-average-power picosecond Yb-doped fiber amplifier," *Optics Letters* **26** (2001)

14. Fabio Di Teodoro and Christopher D. Brooks, "Multistage Yb-doped fiber amplifier generating megawatt peak-power, subnanosecond pulses," *Optics Letters* **30** (2005)

15. Harris, S.E., "Tunable optical parametric oscillators," *Proceedings of the IEEE* **57** (1969)

16. http://www.coherent.com/downloads/SIFIR50_DSrevB.pdf

17. Agrawal, G. P. Fiber-Optic Communication Systems. New York: John Wiley & Sons, Inc, 1997.

18. Agrawal, G. P. Nonlinear Fiber Optics. San Diego: Academic P, 2001.

19. F. Di Teodoro, J. P. Koplow, and S. W. Moore, "Diffraction-limited 300-kW peak-power pulses from a coiled multimode fiber amplifier," *Opt. Lett.* **27** (2002)

20. http://www.thorlabs.com/Images/PDF/Vol18_848.pdf

21. J. Noda, K. Okamoto, and Y. Sasaki, "Polarization-maintaining fibers and their applications," *J. Lightwave Technol.*, **4** (1986)

22. A. Ortigosa-Blanch, J. C. Knight, W. J. Wadsworth, J. Arriaga, B. J. Mangan, T. A. Birks, and P. S. J. Russell, "Highly birefringent photonic crystal fibers," *Opt. Lett.* **25 (**2000).

23. ThorLabs http://www.thorlabs.com/NewGroupPage9.cfm?ObjectGroup_ID=1596

24. http://www.liekki.com/products_detailsYb.php?code=Yb1200-25/250DC-PM

25. ThorLabs http://www.thorlabs.com/NewGroupPage9.cfm?ObjectGroup_ID=910

26. H. Kogelnik and T. Li, "Laser Beams and Resonators," *Appl. Opt.* **5** (1966)

27. Silfvast, William L. Laser Fundamentals: Second Edition. Cambridge, UK: Cambridge University Press, 2004.

28. Yariv, Amnon, and Pochi Yeh. Photonics: Optical Electronics in Modern Communications. Sixth ed. New York: Oxford UP, 2007.

29. Saleh, Bahaa A., and Malvin C. Teich. Fundamentals of Photonics. New York: John J. Wiley & Sons, Inc, 1991.

30. "How to (Maybe) Measure Laser Beam Quality"
    Prof. A. E. Siegman
    Tutorial Presentation at Optical Society of America Annual Meeting (1997)
    (http://www.stanford.edu/~siegman/beam_quality_tutorial_osa.pdf)

31. Richard Lee Sutherland. Handbook of Nonlinear Optics. New York: Marcel Dekker, Inc, 2003, p123

32. Boyd, Robert W. Nonlinear Optics: Second Edition. San Diego: Academic Press, 2003, p74

33. Zayhowski, J. J., "Periodically poled lithium niobate optical parametric amplifiers pumped by high-power passively *Q*-switched microchip lasers" *Opt. Lett.* **22** (1997)

34. Taylor, Henry F. "Bending Effects in Optical Fibers," *Journal of Lightwave Technology* **2** (1984)

35. Digonnet, Michel J.F. Rare-Earth-Doped Fiber Lasers and Amplifiers. 2nd Edition. CRC: New York, 2001

36. A. Smith, B. Do, M. Soderlund, "Deterministic Nanosecond Laser-Induced Breakdown Thresholds in Pure and Yb3+ Doped Fused Silica," *Proc. of SPIE* **6453** (2007)

37. Siegman, A.E., Sasnett, M.W., Johnston, T.F., Jr., "Choice of clip levels for beam width measurements using knife-edge techniques," *Quantum Electronics, IEEE Journal of* , **27** (1991)

38. ThorLabs "Guide to Connectorization, Polishing & Cleaving of Fibers" (Product #: FN96A)

39. http://www.newport.com/file_store/PDFs/tempPDFs/e2888_818-BB-Series-Biased-Detectors.pdf

40. http://www.lecroy.com/shopper/configurequote.asp?prodid=1397

41. http://www.photon-inc.com/PDF/Measuring_Pulsed.PDF

42. A. D'Orazio, M. De Sario, V. Petruzzelli, and F. Prudenzano, "Photonic band gap filter for wavelength division multiplexer," *Opt. Express* **11** (2003)

43. http://www.ozoptics.com/ALLNEW_PDF/DTS0089.pdf

44. P. E. Powers, K. W. Aniolek, T. J. Kulp, B. A. Richman, and S. E. Bisson, "Periodically poled lithium niobate optical parametric amplifier seeded with the narrow-band filtered output of an optical parametric generator," *Opt. Lett.* **23** (1998)

45. P.E. Powers, P.K. Bojja, R. Alkuwari, E. Vershure, and K.L. Schepler, "High energy seeded optical parametric generation with elliptical beams in quasi-phase-matched crystals," *Journal of the Optical Society of America B* **22** (2005)

46. http://www.crystal-fibre.com/datasheets/DC-200-70-PM-Yb-rod.pdf

47. T.A. Birks, J.C. Knight, P. St. J. Russell, "Endlessly single-mode photonic crystal fiber," *Opt. Lett.* **22** (1997)

48. J.R. Folkenberg, M.D. Nielsen, N.A. Mortensen, C. Jakobsen, and H.R. Simonsen, "Polarization maintaining large mode area photonic crystal fiber," *Opt. Express* **12** (2004)